Histone H2A.Z Deacetylation and Dedifferentiation in Infarcted/Tip60-depleted Cardiomyocytes

Xinrui Wang[1,3], Katherine Kulik[2,3], Tina C. Wan[1,3],
John W. Lough[2,3*], John A. Auchampach[1,3*]

[1]Department of Pharmacology and Toxicology
[2]Department of Cell Biology Neurobiology and Anatomy
[3]Cardiovascular Center
Medical College of Wisconsin
Milwaukee, WI 53226

*Co-corresponding authors

Number of Figures: 8

Number of Tables: 0

Number of Supplemental Figures: 9

Number of Supplemental Tables: 1

Key Words: Cardiomyocyte, CUT&Tag, Dedifferentiation, Histone H2A.Zac$^{K4/K7}$, RNAseq, Tip60

Financial Support: NHLBI 5R01HL131788 (JAA & JWL) and American Heart Association 24CDA1268289 (XW).

Running Title: H2A.Z deacetylation/dedifferentiation in Tip60-depleted cardiomyocytes

Co-Corresponding Authors: John A. Auchampach, PhD
Department of Pharmacology & Toxicology
Medical College of Wisconsin
Milwaukee, Wisconsin 53226
Email: jauchamp@mcw.edu

John W. Lough, PhD
Department of Cell Biology, Neurobiology & Anatomy
Medical College of Wisconsin
Milwaukee, Wisconsin 53226
Email: jlough@mcw.edu

Non-Standard Abbreviations: CM, cardiomyocyte; cTnT, cardiac troponin-T; H2A.Zac$^{K4/K7}$, histone H2A.Z acetylated at lysines 4 and 7; *Kat5*, *lysine acetyltransferase-5* (Tip60); Tip60 KO, *Kat5* gene knockout; MI, myocardial infarction; Tip60, Tat-interactive protein 60 kD; WGA, wheat germ agglutinin

Author Contributions: XW, JWL, and JAA designed the study. XW, KK, and TCW performed the experiments. XW, JWL, and JAA analyzed data, prepared figures, and wrote the manuscript. All authors reviewed, revised, and approved the final version.

Conflicts of Interest: none declared.

ABSTRACT

Myocardial infarction (MI) results in the loss of billions of cardiomyocytes (CMs), resulting in cardiac dysfunction. To re-muscularize injured myocardium, new CMs must be generated via renewed proliferation of surviving CMs. Approaches to induce proliferation of CMs after injury have been insufficient. Toward this end we are targeting the acetyltransferase Tip60, encoded by the *Kat5* gene, based on the rationale that its pleiotropic functions combine to block CM proliferation at multiple checkpoints. We previously demonstrated that genetic depletion of Tip60 in a mouse model after MI reduces scarring, retains cardiac function, and activates the CM cell-cycle, although it remains unclear whether this culminates in the generation of daughter CMs. In order for pre-existing CMs in the adult heart to undergo proliferation, it has become accepted that they must first dedifferentiate, a process highlighted by loss of maturity, epithelial to mesenchymal transitioning (EMT), and reversion from fatty acid oxidation to glycolytic metabolism, accompanied by softening of the myocardial extracellular matrix (ECM). Based on recently published findings that Tip60 induces and maintains the differentiated state of hematopoietic stem cells and neurons via site-specific acetylation of the histone variant H2A.Z, we assessed levels of acetylated H2A.Z and dedifferentiation markers after depleting Tip60 in CMs post-MI. We report that genetic depletion of Tip60 from CMs after MI results in the near obliteration of acetylated H2A.Z in CM nuclei, accompanied by the altered expression of genes indicative of EMT induction, ECM softening, decreased fatty acid oxidation, and depressed expression of genes that regulate the TCA cycle. In accord with the possibility that site-specific acetylation of H2A.Z maintains adult CMs in a mature state of differentiation, CUT&Tag revealed enrichment of H2A.Zac$^{K4/K7}$ in genetic motifs and in GO terms respectively associated with CM transcription factor binding and muscle development/differentiation. Along with our previous findings, these results support the notion that Tip60 has multiple targets in CMs that combine to maintain the differentiated state and prevent proliferation.

INTRODUCTION

The burden of ischemic heart disease remains large, with myocardial infarction (MI) and heart failure accounting for nearly 15% of deaths in the U. S.[1] Because billions of cardiomyocytes (CMs) are lost during MI, the goal of protecting and re-muscularizing the myocardium constitutes an urgent clinical challenge. The mitigation of cardiac dysfunction caused by CM loss and replacement by scar tissue after MI requires the regeneration of lost CMs, i.e. re-muscularization. Unlike most organs, the adult heart cannot generate replacement CMs because these cells have evolved to reside in a profound state of proliferative senescence that becomes established soon after birth.

With the goal of releasing surviving CMs from their non-proliferative state, research during the past decade has targeted proteins that either induce or inhibit CM proliferation, via the respective over-expression or knockout (KO) of genes in mouse models (reviewed in [2]). Although these studies have shown that the CM cell-cycle can be re-activated when targeting individual genes, extent of proliferation and functional improvement in most cases is minimal, which is not surprising considering the array of inhibitors that prevent CMs from dividing. In order to disengage this inhibitory network following MI, we are targeting the Tip60 acetyltransferase, per a rationale based on findings in cultured cell-lines showing that Tip60 is pleiotropic, acetylating proteins that block the cell-cycle at three checkpoints: (i) G_1/S, by maintaining p21 at inhibitory levels [3, 4], (ii) G_2/M, by activating Atm to induce the DNA damage response (DDR; [5]), and (iii) cytokinesis, via acetylation of Aurkb [6]; also, because Tip60-mediated acetylation of p53 induces apoptosis [7-9], its targeting may be cardioprotective. Consistent with these *in vitro* findings, our recent work using an *in vivo* Tip60 KO model has shown that genetic depletion of Tip60 from CMs after MI restores systolic function to near pre-MI baseline levels, with reduced apoptosis and scarring accompanied by cell-cycle activation [10, 11], and that these benefits are phenocopied by administering drugs designed to inhibit Tip60's acetyltransferase activity [12]. However, it remains unclear whether activation of the CM cell-cycle results in bona fide proliferation, i.e. the generation of daughter CMs that are mononuclear and diploid, fulfilling a major challenge in the field of cardiac regeneration.

It has recently become accepted that for mature CMs in the injured adult heart to resume proliferation, they must first undergo dedifferentiation [13-19], a phenomenon wherein the expression of adult cardiac genes becomes diminished as embryonic genes are re-expressed (reviewed in [20-23]). CM dedifferentiation is highlighted by cell-cycle activation [13-15], epithelial-to-mesenchymal transition (EMT; [16]), softening of the myocardial extracellular matrix (ECM) [15, 17, 24-26], and, as recently reported, inhibition of fatty acid oxidation [18]. Here, we report that Tip60 KO in CMs is accompanied by the near-complete loss of acetylation of lysines K4 and K7 in the histone variant H2A.Z, hereafter denoted H2A.Zac$^{K4/K7}$, a Tip60-mediated epigenetic modification recently shown to be required to maintain the differentiated state in hematopoietic stem cells (HSCs [27]) and neurons [28]. We accordingly show that H2A.Zac$^{K4/K7}$ is enriched in genetic motifs and GO terms associated with CM transcription factor binding and muscle development/differentiation, respectively, and that Tip60 KO alters the expression of genes which regulate CM dedifferentiation. Interpreted in accord with our previous findings [10, 11], these results indicate that depletion of Tip60 after MI permits the resumption of CM proliferation by initiating dedifferentiation, as well as by surmounting cell-cycle blockade. These findings provide further support for the possibility that clinical targeting of Tip60 could promote myocardial regeneration post-MI.

MATERIALS AND METHODS

Animal Care & Experimentation: These experiments adhered to the National Institutes of Health (NIH) Guide for the Care and Use of Laboratory Animals (NIH Pub. Nos. 85-23, Revised 1996). All protocols are described in an Animal Use Application (AUA #000225) approved by the Medical College of Wisconsin Institutional Animal Care and Use Committee (IACUC), which possesses Animal Welfare Assurance status from the Office of Laboratory Animal Welfare (A3102-01).

Preparation of the mouse model used in these experiments wherein exons 3-11 of the *Kat5* gene encoding Tip60 are floxed, comprising two-thirds of the coding sequence including the chromo and acetyltransferase domains, was previously described [29]. These mice were mated with mice containing an α-myosin heavy chain (*Myh6*)-driven *MerCreMer-recombinase* transgene (Jackson Laboratory #005650), the Cre recombinase product of which, upon administration of tamoxifen, translocates from the cytoplasm to the nucleus to recombine floxed alleles [30]. All mice were on a mixed B6/sv129 genetic background. Experimental groups contained equal numbers of adult (10-14 weeks-old) males and females.

To ablate floxed *Kat5* alleles, mice received a daily intraperitoneal injection of tamoxifen (40 mg/kg [Sigma #T5648] suspended with 5% ethanol in sunflower oil) for three consecutive days. In experiments involving myocardial infarction (MI; described in detail below), tamoxifen was intra-peritoneally administered on three consecutive days, beginning on the third day after inducing MI via ligation of the left main coronary artery. On the day of harvest (i.e. 14 days post-MI and 11 days after the first injection of tamoxifen), mice were euthanized with CO_2, followed by removal of hearts and processing components for isolating total RNA, for which tissue between the base and ~1 mm above the suture was utilized, and immunostaining/protein isolation, for which tissue ~1 mm above the suture to the apex was utilized. Tissue samples for RNA and protein isolation were respectively placed in TRIzol (Thermo-Fisher #15596026), and Histone Extraction Buffer (Active Motif #37513) containing Halt's protease/phosphatase inhibitor cocktail (Thermo-Fisher #78440) with deacetylase inhibitors (MedChemExpress #HY-K0030), minced, homogenized with a teflon pestle, and stored at -80° C until further processing.

Myocardial Infarction: To induce MI, mice were anesthetized with isoflurane (1.0-1.5%) delivered via a nose cone, intubated and mechanically respirated (model 845, Harvard Apparatus) via an endotracheal tube with room air supplemented with 100% oxygen; to maintain anesthesia, isoflurane was delivered via the ventilator. The electrocardiogram (ECG; limb lead II configuration) was continuously recorded (Powerlab) using needle electrodes; rectal temperature was maintained at 37°C throughout the experiments using a servo-controlled heating pad. Before initiating surgery, mice were subcutaneously injected with sustained release meloxicam (4 mg/kg) to limit post-operative pain. Once anesthetized, thoracotomy was performed to the left of the sternum to expose the heart. This was followed by opening the pericardium, and, with assistance of a microscope, insertion of an 8.0 nylon suture beneath the left main coronary artery at a level below the tip of the left atrium; this placement was designed to target the lower half of the ventricle. Ischemia was then induced by ligating the suture with a double knot, after which coronary occlusion was verified by observation of myocardial blanching distal to the ligature, as well as by ST segment elevation per ECG. Following ligation, the chest wall was closed with polypropylene suture, and recovery was monitored until mice became fully ambulatory.

Genotyping: Genotyping was performed by PCR in 20 µl volume reactions that included 1x GoTaq Green Master Mix (Promega #M7123), 1.1 mM $MgCl_2$, 0.5 µM each primer, 0.5 µM internal control primers, and 4.0 µl template. Templates were from supernatants of ear tissue that had been boiled for 10 minutes in 0.3 mL 10 mM NaOH/1 mM EDTA. Sequences of primer pairs employed for PCR are listed in Supplemental Table 1. PCR products were amplified in an AB Applied Biosystems GeneAmp PCR System 9700 using the following programs: for LoxP, one 5-minute cycle at 95° C, thirty-five cycles at 94° C 30 sec/61° C 45 sec/72° C 45 sec, followed by one 10-minute cycle at 72° C; for *Myh6-MerCreMer*, one 5-minute cycle at 95° C, thirty-five cycles at 94° C 30 sec/54° C 45 sec/72° C 45 sec, followed by one 10-minute cycle at 72° C. Amplicons were separated at 100-110 V for one hour in 1% agarose/ethidium bromide and imaged.

RT-qPCR: Heart tissue, previously disrupted by homogenization with a motorized (Kimble 749540-0000) Teflon pestle and stored at -80° C in TRIzol reagent, was thawed. RNA was immediately purified using PureLink RNA

Mini-Kits (ThermoFisher #12183018A), including a genomic DNA removal step (PureLink DNase kit for on-column protocol, Thermo-Fisher #12185-010), according to the manufacturer's instructions. RNA yield & quality were determined via 260/280 ratio using Eppendorf Biophotometer Plus Instrument.

cDNA was synthesized as follows. After diluting an RNA sample from each heart so that precisely 1.0 µg was suspended in 14 µl nuclease-free distilled water (NFDW), 4.0 µl 5x VILO reaction mixture (ThermoFisher #11754050) were added. To start the reverse-transcription reaction, 2.0 µl 10x SuperScript Enzyme Mix (ThermoFisher #11754050) were added, followed by transfer to an Applied Biosystems Veriti 96-well Thermocycler programmed as follows: 10 minutes at 25° C, 60 minutes at 42° C, and 5 minutes at 85° C. cDNA templates were diluted with NFDW to a concentration of 3.125 ng/µl and stored at -20° C.

qPCR was carried-out by subjecting each biological replicate (i.e., sample from each individual heart) to triplicate determinations. Each reaction was performed in a total volume of 10 µl in 384-well arrays, each well containing 1x Taqman Fast-Advanced Master Mix (ThermoFisher #4444557), 1x Taqman Probe Kit (Supp. Table 1), and 12.5 ng cDNA as template. The arrayed samples were amplified in a Bio-Rad CFX384 Real Time System (C1000 Touch) programmed as follows: 2 minutes at 50° C, 20 seconds at 95° C, 3 seconds at 95° C, and 30 seconds at 60° C; the last two steps were repeated 39 times. Results were processed using Bio-Rad CFX Manager 3.1 software.

Western Blotting: Histones were purified from adult heart tissue using Active Motif's Histone Purification Mini Kit (cat. no. 40026), according to the manufacturer's recommendations which were modified as described below. All procedures were performed at 0-4 °C. Using a minimal volume of low pH Extraction Buffer, which contains protease and deacetylase inhibitors, 50mg tissue was completely dispersed using a Dounce homogenizer and a microtip sonicator, followed by centrifugation (5 min, 21,000g). Following adjustment of the supernatant to pH8.0 using 5X Neutralization Buffer, 'crude' histones were de-salted using a Zeba Spin Desalting Column (Thermo-Fisher #89883), after which sample buffer (Cell Signaling Technology #12957) was added. For electrophoresis, a sample from each heart was loaded into individual lanes of a pre-cast Bio-Rad 4-20% acrylamide gel. After application of current (100 V) until the tracking dye reached the bottom of the gel, separated proteins were transferred (60 min at 100 V) onto 0.2 µm nitrocellulose membrane (Thermo-Fisher #88013). Blots were blocked with 5% non-fat dry milk/20 mM Tris (pH 7.6)/150 mM NaCl/0.1%Tween-20 (5% NFDM/TBST) or 5% BSA in TBST. Primary and secondary antibodies and dilutions are acetyl-histone H2A.Z (Lys4/Lys7, 1:1000, Cell Signaling Technology D3V1I, cat. no. #75336), histone H2A.Z (1:1000, Active Motif AB_2615081, cat. no. #39013), and HRP-linked goat anti-rabbit (1:2000, Cell Signaling Technology #7074). Blots were reacted with primary antibody in 5% NFDM/TBST or 5% BSA/TBST overnight at 4°C. Secondary antibodies were diluted in 5% BSA/TBST and applied for 60 minutes at RT. Reacted blots were covered with Pierce™ ECL horseradish peroxidase substrate (ThermoFisher #32209) for 1 min at room temperature, followed by chemiluminescence imaging and densitometry using Bio-Rad ChemiDoc and ImageJ software, respectively.

Immunostaining & Cell Counting: On the day before harvest, mice were injected with 1 mg 5'-bromo-2'-deoxyuridine (BrdU; Sigma #B9285). Following removal, hearts were perfused with ice-cold cardioplegic solution and atria were removed. Ventricles were fixed overnight in fresh ice-cold 4% paraformaldehyde/PBS, processed through ethanol series, and embedded in paraffin. Sections (4 µm thick) mounted on microscope slides were de-waxed, subjected to antigen retrieval (100°C in 10 mM trisodium citrate pH6.0/0.05% Tween-20 for 20 minutes) followed by 30 minutes' cooling at RT, and blocked with 2% goat or 5% donkey serum/0.1% Triton-X-100 in PBS. Primary antibodies against acetyl-histone H2A.Z (Lys4/Lys7, 1:100, Cell Signaling Technology D3V1I, cat. no. #75336), histone H2A.Z (1:200, Active Motif AB_2615081, cat. no. #39013), Nkx2.5 (1:250, Abcam #ab106923), cardiac Troponin-T (cTnT, 1:2000, Abcam #ab8295), α-smooth muscle actin (α-SMA, 1:100, Dako #M0851), and H3K4^{me3} (1:600, Active Motif #39160) were diluted in blocking buffer and applied overnight at 4°C; secondary antibodies goat anti-rabbit 568 (1:500, Invitrogen #A-11036), goat anti-mouse 488 (1:500, Invitrogen #A-11029), donkey anti-rabbit 555 (1:500, Invitrogen #A-31572), and donkey anti-goat 488 (1:500, Invitrogen #A-32814) were applied for one hour in the dark.

Microscopy was performed using a Nikon Eclipse 50i microscope equipped with a Nikon DSU3 digital camera. During counting, at least 300 CMs were evaluated in 6 random 400x photomicrographic fields, identity of which were confirmed by immunostaining the cytoplasmic marker cardiac troponin-T (cTnT) or the nuclear marker Nkx2.5. Percentages of CMs expressing acetylated or bulk histone H2A.Z were assessed by monitoring fluorescent signal in the Texas Red channel, after confirming the identity of each stained CM in the FITC channel.

To identify nuclei as acetylated or bulk histone H2A.Z -positive, only those at least half-filled with fluorescence were counted; acetylated or bulk histone H2A.Z positive nuclei were also confirmed to be DAPI-positive. In infarcted hearts, acetylated or bulk histone H2A.Z immunoreactivity were assessed in both the remote zone, specifically the area of myocardium ~2 mm distal to the infarct boundary, and in the border zone, specifically the area immediately adjacent to the infarct zone. WGA staining was performed using Thermo-Fisher #W11263 Alexa Fluor 350 conjugate.

RNAseq: RNA quality was determined using an Agilent BioAnalyzer 2100. RNA libraries were prepared by BGI Americas. Samples were tested for strand-specific mRNA sequencing on a DNBSEQ platform. SOAPnuke v1.5.2 was used to remove reads whose N content is greater than 5%, the reads containing the adaptor, and reads with low base quality (< 15). Filtered clean reads (>45 M per sample) were stored in FASTQ format and aligned to the *Mus musculus* genome (GCF 000001635.26 GRCm38.p6) using HISAT2 v 2 0.4. Bowtie2 was used to align clean reads to the reference genes. A total of 17,714 genes were detected. The average alignment ratio of the sample comparison genome was 96.63%. Gene expression levels were calculated by RSEM (v1.2.28) and quantified by fragments per kilobase of transcript per million reads mapped (FPKM). DEGs for each experimental group, as compared to control, were detected using DESeq2. The phyper function in R software is used for enrichment analysis and calculation of P values; Q values were obtained by correction of the P value.

Cleavage Under Targets & Tagmentation Assay (CUT&Tag): Approximately ten milligrams of left ventricular tissue micro-dissected from three non-infarcted wild-type (WT) hearts of 14 week-old adult mice not treated with tamoxifen were processed for CUT&Tag using the Active Motif tissue kit (cat. #53170). Briefly, 10^6 nuclei isolated from each heart were attached to Concanavalin A beads and incubated overnight with either anti-H2A.Zac$^{K4/K7}$ antibody (rabbit mAb: Cell Signaling Technology D3V1I, cat. no. 75336) or anti-bulk H2A.Z antibody (rabbit pAb: Active Motif AB_2615081, cat. no. 39113), followed by attachment to guinea pig secondary anti-rabbit antibody provided in the kit. Antibody-bound targets were subjected to cleavage and tagmentation via incubation with protein-A-Tn5 transposase/sequencing adapters, followed by DNA purification, PCR amplification using a unique i7/i5 primer pairs for individual samples, and isolation on SPRI beads. DNA libraries were sequenced on Illumina NextSeq 550 (8 million reads, 38 paired-end). For additional details see instructions in Active Motif CUT&Tag-IT kit #53170. Fraction of Reads In Peaks (FRIP) percentages ranged from 36.8 to 43.9, with total peak numbers ranging from 34,810 to 53,327. Peak annotation and motif analysis were assessed using HOMER [31]. Across all three samples, upset plotting revealed a consensus set of ~30,000 peaks. H2A.Zac$^{K4/K7}$ tracks in selected genes were imaged using the WashU Epigenome Browser [32] (https://epigenomegateway.wustl.edu/browser).

Statistics: The DEG heatmap was generated by the Dr.Tom platform (BGI Americas) according to the DESeq2 analysis results. GO enrichment analysis of annotated DEGs was performed by Phyper based on Hypergeometric test. The significant levels of terms and pathways were corrected by Q value with a rigorous threshold (Q value ≤ 0.05). All other determinations were performed in blinded fashion and are reported as means ±SEM, and compared by an unpaired, two-tailed Student's t test. $P<0.05$ was considered statistically significant.

RESULTS

Genetic Depletion of Tip60 in CMs Abolishes Acetylation of Histone H2A.Z.

In this study we compared 12 week-old adult control mice denoted *Kat5*$^{f/f}$ (i.e., *Kat5*$^{flox/flox}$) with experimentals designated *Kat5*$^{\Delta/\Delta}$ (i.e., *Kat5*$^{flox/flox;Myh6\text{-}merCremer}$), in which the *Kat5* gene encoding Tip60 was disrupted by injecting tamoxifen for three consecutive days to activate *Myh6*-driven Cre-recombinase. In infarcted hearts treated with tamoxifen for three days beginning on the third day post-MI (hereafter 'infarcted/Tip60-depleted' hearts), expression of the *Kat5* gene assessed at the tissue level was reduced ~25%; since Cre is only expressed in CMs, reduction was presumably more extensive at the CM level; by contrast, *Kat5* expression was unaffected in control hearts to assess off-target effects of Cre-recombinase (Supp. Fig. 1a). Using this model we recently reported that depletion of Tip60 after MI preserves cardiac function, reduces scarring, and re-initiates the cell-cycle in CMs of both neonatal [10] and adult hearts [11]. Here, as shown in Figure 1a, depletion of Tip60 (*Kat5*$^{\Delta/\Delta}$) in CMs of infarcted adult hearts resulted in the absence of H2A.Zac$^{K4/K7}$ in nearly all CM nuclei. This was the most pronounced effect of Tip60 depletion that we have observed, in this as well as in our previous studies [10-12]. To verify that depletion of H2A.Zac$^{K4/K7}$ was confined to CM nuclei, CM identity was confirmed by immunostaining the nuclear marker Nkx2-5 (Supp. Fig. 2). By contrast, using an antibody that detects bulk (i.e., both acetylated and non-acetylated) H2A.Z, no effects of Tip60 depletion were seen (Supp. Fig. 3). Surprisingly, the percentage of H2A.Zac$^{K4/K7}$-positive nuclei of interstitial cells (i.e., non-CMs) was increased in both the infarct border and remote zones (Supp. Fig. 4). CM-specific depletion of H2A.Zac$^{K4/K7}$ did not represent an off-target effect of Cre-recombinase (Supp. Fig. 5). We performed western blotting to verify reduction of H2A.Zac$^{K4/K7}$ in Tip60-depleted in CMs. As shown in Figure 1b, despite blotting total proteins extracted from whole heart tissue wherein most cells are non-CMs, H2A.Zac$^{K4/K7}$ levels were markedly reduced by ~two-thirds when Tip60 was depleted, even though levels of bulk H2A.Z were modestly increased (Supp. Fig. 6).

Infarcted/Tip60-depleted Hearts Display Dysregulation of Genes Associated with CM Dedifferentiation & Cell-Cycle Activation.

Based on findings that Tip60-mediated acetylation of H2A.Z sustains differentiation in HSCs [27] and neurons [28], combined with reports that adult CMs undergo dedifferentiation in order to permit resumption of cell-cycling and regeneration after myocardial injury [14-16, 19, 33], it was of interest to assess whether reduced levels of H2A.Zac$^{K4/K7}$ in CMs correlated with the altered expression of markers commonly associated with the dedifferentiation process. Hence, we assessed the effects of depleting Tip60 in CMs using RNAseq, which revealed global effects in both naive and infarcted hearts, respectively highlighting 3,242 and 4,049 differentially expressed genes, (DEGs) with only minimal effects (88 DEGs) of Cre-recombinase (Supp Fig. 1b-c).

We previously reported that the S- and G_2-phase regulators *Ccna2*, *Ccnb1* and *Cdk1* are increased 2-3 fold in infarcted/Tip60-depleted adult heart [11]. In the present study, RNAseq confirmed and extended these findings, revealing increased expression of the pro-proliferative genes *Top2a, Kif23, Mki67, Bub1, Prc1, Stmn1* (Fig. 2b) in infarcted/Tip60-depleted hearts, all of which are reportedly up-regulated in a proliferating subpopulation of CMs within the adult heart [34]. In addition, our RNAseq (Fig. 2c) and corroborating RT-qPCR (Fig. 2d) data showed that depletion of Tip60 was associated with the up-regulation of genes encoding Dab2, and Runx1, previously shown to be induced by oncostatin-M (Osm) at the onset of CM dedifferentiation [13, 14]; accordingly, increased expression of genes encoding Osm and its receptor (Osmr) was also noted. *Fgfr1* and *Tgfbr1*, which have been associated with CM dedifferentiation [15], were also increased in Tip60-depleted hearts, as well as *Tgfb3* (Fig. 2c-d). However *Fgf1*, which among members of the large Fgf family is selectively expressed in CMs [35], was decreased (Figs. 2c-d; Fig 4a). Although controls to assess effects of Cre recombinase (Fig. 2a) suggested increases in GO terms that were reduced by Tip60 KO, none were statistically significant; also, Cre had no effects on any of the genes evaluated in Figures 2b-d.

Altered Expression of Genes Indicative of EMT Transitioning & Cytoskeletal Disassembly in Infarcted/Tip60-depleted Hearts

Dedifferentiating CMs undergo a partial epithelial to mesenchymal (i.e. EMT-like) transition [16, 36], accompanied by disassembly of the cytoskeleton/sarcomere complex [37] (reviewed in [23]). As shown in Figure 3a, >75% of genes in the EMT GO Term were upregulated in infarcted/Tip60-depleted hearts, consistent with findings by others that CM dedifferentiation induced by over-expression of *Erbb2* is accompanied by up-regulation of EMT-like genes [16], among which 28 were up-regulated subsequent to Tip60 KO (Fig. 3b). Per Fig. 3c, RT-qPCR confirmed up-regulation of the EMT genes *Gja1*, *Myocd*, *Myc*, and *Tbx20*, as well as the following 'EMT-like' genes: *Actn1*, which encodes α-Actinin and is normally expressed in developing CMs and in destabilized adult CMs [37]; *Cttn*, which encodes the actin-binding protein cortactin and promotes lamellipodia formation in migrating cells [38-40]; and *Nes,* which encodes the intermediate filament protein nestin in embryonic CMs [41] and was recently shown to be increased in dedifferentiating CMs [16].

Among genes associated with cytoskeletal disassembly, *Mapt* was of interest because it not only encodes Tau to maintain microtubule stability, but also because its expression during neurogenesis is dependent upon Tip60 [28]. Accordingly, RNAseq indicated that expression of *Mapt*, which is selectively expressed in CMs [35], was reduced by Tip60 KO (Fig. 3d). Other depressed cytoskeletal genes include *Mylk4*, a CM-specific kinase that maintains the myofilament [42, 43], *Myom1* (myomesin-1), a CM dedifferentiation marker [13, 20] that maintains the thick filament, and *Acta2* (smooth muscle actin), which is reportedly decreased [16] as well as increased [13, 15] during dedifferentiation. Regarding *Acta2*, these disparate findings may be reconciled because decreased expression was detected by RT-qPCR/RNAseq of whole heart tissue (Fig. 3b-d & ref. [16]), whereas increased expression was seen by western blotting of isolated CMs, and by immunostaining [13, 15], the latter being consistent with our immunostaining results showing that α-SMA, which is expressed in CMs only at the earliest stages of heart development [44], is re-expressed in border zone CMs in infarcted/Tip60-depleted hearts (Supp. Fig. 7). Regarding up-regulated markers, it is noteworthy that *Cdk1* has been reported to regulate sarcomere disassembly [37] and that *Shroom 3* has been shown to regulate polarity and cytoskeletal organization [45] (Fig. 3c-d). Most importantly and in accord with recent findings [46, 47], effects on expression of the genes encoding embryonic (*Tnni1*) and adult (*Tnni3*) isoforms of troponin I indicated that Tip60 KO induced a transition toward the immature dedifferentiated state (Fig.3c-d).

Increased Expression of 'Soft' ECM Genes in Infarcted/Tip60-depleted Hearts

As the heart develops, the extracellular matrix (ECM) transitions from softness to rigidity, based on relative abundance of collagen 4, emilin-1, fibronectin and periostin at immature stages, followed by higher levels of collagen-1, collagen-3 and laminin at adult stages [25]. ECM softness positively correlates with the ability of CMs to proliferate [17]. To enable CM proliferation in the adult heart, CMs must be able to migrate, requiring a metalloproteinase-induced transition from rigid to soft ECM [48, 49 50]. Indicative of softening, Tip60 KO increased expression of genes in the GO Term 'Extracellular Matrix' (Fig. 4a), as well as genes associated with soft ECM including *Col4a1, Col4a2, Emilin1*, *Fn1*, and *Postn* (Fig. 4b-c); periostin (*Postn*), which was strongly increased, promotes CM proliferation and cardiac repair [51]. Per Figure 4c, genes associated with Erbb2-induced CM dedifferentiation [36] – *Fn1*, *Loxl2, Col3a1*, *Col4a2*, *Col6a1*, *Col8a2*, *Col15a1* – were also increased, among which *Col15a1* is required for matrix remodeling and CM proliferation [52-54]. Tip60 KO also increased expression of ECM genes associated with Fgfr1/Osmr-induced dedifferentiation [15], including *Col8a1*, *Emilin-1*, *Timp1*, and *Agrn* (agrin), which promotes cardiac regeneration post-MI [24, 55]. Genes increased in both Erbb2- [36] and Fgfr1/OsmR-induced [15] CM dedifferentiation were also increased – *Col1a1, Col4a1, Ctgf, Mmp2, Postn,* and *Vcan* – the latter of which supports CM migration [56]. The most strongly up-regulated ECM component in the Tip60-depleted heart was *Cthrc1* (>11-fold), encoding collagen triple helix repeat containing-1 [57], which is required for ECM reconstruction after myocardial injury [58 59]. These findings support the notion that depletion of Tip60 post-MI induces matrix softening to permit CM migration and proliferation.

Altered Metabolic Programming in Infarcted/Tip60-depleted Hearts

Transition to CM maturity is accompanied by a metabolic change from glycolysis to fatty acid oxidation (FAO) (review, [60]). After MI, the ability of CMs to re-enter the cell-cycle requires reversion to glycolysis[15, 16, 18, 61]. Tip60 KO affected the expression of genes regulating FAO, TCA cycle, and glycolysis (Figs. 5-7). Per Figure 5a, although Cre (*Kat5*$^{+/+;merCremer}$) mildly reduced expression of some genes in the GO Term FAO, Tip60 KO strongly suppressed nearly all FAO genes, including genes that regulate breakdown of short- thru very long-chain fatty acids, i.e. *Acads, Acadm, Acadl,* and *Acadvl* (Fig. 5b). Reduced expression of carnityl palmitoyltransferase 1B (*Cpt1b*), which governs the rate-limiting step in FAO, is particularly noteworthy because its depletion in CMs was recently shown to induce dedifferentiation and renewed proliferation [18].

Regarding Krebs Cycle genes, despite downward trends caused by Cre (Fig. 6a), Tip60 KO strongly reduced the expression of genes in families regulating each step of the cycle (Fig. 6b-c). Among these, genes encoding succinate dehydrogenase (Sdh) isoforms, especially *Sdhb*, *Sdhc* and *Sdhd*, were strongly reduced, which is noteworthy because inhibition of Sdh after MI promotes CM proliferation and revascularization[62]. An exception to the reduced expression of TCA cycle genes was the absence of an effect on *α-ketoglutarate dehydrogenase* (*Ogdh*), which is notable because its targeted disruption increases cell-cycle activation and numbers of CMs [18, 63]; it is speculated that this reflects a compensatory response to prevent CM proliferation.

Because genes regulating Fatty Acid β-Oxidation (Fig. 5) and the TCA Cycle (Fig. 6) were reduced by Tip60 KO, it was anticipated that a pronounced reversion to glycolysis would be observed. However, although genes governing crucial glycolytic steps, including *Hk1* encoding the rate-limiting enzyme hexokinase-1, were up-regulated, most genes in the glycolytic GO term were decreased (Fig. 7a). Nonetheless, isoforms in glycolytic gene families which are normally modestly expressed – *Slc2a1*, *Slc16a3*, *Slc16a7*, *Pfkl*, *Eno1*, *Eno2*, *Pdk3*, *Ldha* – were significantly up-regulated (Fig. 7b-c).

Enrichment of H2A.Zac$^{K4/K7}$ in Cardiomyocyte Maturity Genes

Because specific depletion of Tip60 in CMs nearly obliterates acetylation of H2A.Zac$^{K4/K7}$ (Fig. 1) and causes dedifferentiation (Figs. 2-7), we are assessing whether H2A.Zac$^{K4/K7}$ is enriched in cardiac maturity genes, akin to its association with genes that confer maturity of HSCs [27] and neurons [64]. Toward this end we are performing CUT&Tag using the anti-H2A.Zac$^{K4/K7}$ antibody employed in Figure 1; although this antibody was previously qualified for CUT&Tag on U2OSg1/C9 cells [65], we qualified it for use on nuclei isolated from adult heart tissue by comparing peaks obtained with anti-bulk H2A.Z, which was previously qualified on nuclei from heart tissue by the manufacturer. As shown in Supp. Fig. 8a, comparison of targets identified by each antibody revealed an average Pearson Correlation of ~0.86, indicating efficient detection of H2A.Zac$^{K4/K7}$. Peak annotation indicated that 15-23% of H2A.Zac$^{K4/K7}$ peaks were in promoter-TSS loci (Supp. Fig. 8b), and, consistent with a role in CM maturation, H2A.Zac$^{K4/K7}$ was enriched in cardiac transcription factor binding motifs (Fig. 8a) and in gene ontology (GO) terms denoting cardiomyogenesis (Fig. 8b). Genome browsing revealed that promoter and upstream loci of the *Tnni3* gene, expression of which has been considered to be cardinal indicator of CM maturity [46, 47], were enriched in H2A.Zac$^{K4/K7}$ relative to loci in the gene encoding the immature isoform *Tnni1* (Fig. 8c); accordingly, expression of *Tnni3* and *Tnni1* were respectively decreased and increased by KO of *Kat5* (Fig. 3c-d), indicative of CM dedifferentiation. Using CUT&Tag, we are following-up these findings to co-localize H2A.Zac$^{K4/K7}$ with factors including H3K4^{me3}, H3K27^{me3}, and Ub-H2B, which have been implicated in the regulation of CM maturity genes[18, 47, 63, 64], in the presence and absence of Tip60; in this regard it is noteworthy that levels of H3K4^{me3} and Ub-H2B were modestly but significantly reduced in CM nuclei of Tip60-depleted hearts (Supp. Fig. 9).

In summary, considered within the context of findings reported in other cell types[27, 64, 65, 72-78], results in Figures 1-8 support the notion that site-specific acetylation of the histone variant H2A.Z by Tip60 is required to maintain the expression of genes that drive CM differentiation and maturation.

DISCUSSION

Resume: Our recently published findings support the hypothesis that genetic depletion [10, 11] or pharmaceutical inhibition [12] of the pleiotropic acetyltransferase Tip60 (*Kat5*) after myocardial infarction (MI) confers cardioprotection and regeneration by preventing the site-specific acetylation and activation of targets that are pro-apoptotic (i.e., p53) and anti-proliferative (i.e., Atm). We extend these findings here by showing that post-MI depletion of Tip60 nearly obliterates site-specific acetylation of the histone variant H2A.Z (i.e. H2A.Zac$^{K4/K7}$) in CMs, a chromatin target associated with induction and maintenance of the differentiated state in other cells. Specifically, western blotting indicated that depletion of Tip60 post-MI reduced levels of H2A.Zac$^{K4/K7}$ in heart tissue by approximately two-thirds (Fig. 1b), and, most remarkably, immunostaining revealed near-obliteration of H2A.Zac$^{K4/K7}$, specifically in CM nuclei (Fig. 1a). We speculate that retention of H2A.Zac$^{K4/K7}$ in ~30% of CM nuclei within the border zone of infarcted hearts reflects inability of tamoxifen, when administered three days after MI, to perfuse this region due to vascular injury, and/or perhaps increased levels of Tip60 in infarcted hearts observed in preliminary findings.

Obliteration of H2A.Zac$^{K4/K7}$ was concomitant with dedifferentiation (Figs. 2-7), a process now considered as prerequisite for the ability of CMs to undergo cell-cycle reactivation and bona fide proliferation to effect myocardial regeneration [13-17, 23, 79-81]. This result is consistent with recent findings that Tip60-specific acetylation of H2A.Z is required to maintain the differentiated state of hematopoietic stem cells (HSCs)[27], and neurons [28]; because these reports showed that acetylated H2A.Z binds pioneer transcription factors that activate genes to establish cellular maturity – specifically Myc in HSCs [27] and Ascl1 in neurons [28] – it will be of extraordinary interest to ascertain whether H2A.Zac$^{K4/K7}$ recruits cardiomyogenic transcription factors, consistent with findings in Figure 8a, to enhancer/promoter loci of genes that maintain the CM differentiated state. The interesting possibility that acetylation of H2A.Z is required to specify all cell-types is suggested because earlier findings (that did not consider a role for Tip60) showed that H2A.Z acetylation is required for skeletal [74] and smooth [76] muscle cell differentiatiion. A crucial role for Tip60 in maintaining H2A.Z genetic loci is indicated by recently published findings showing that disruption of the NuA4/Tip60 complex in K562 cell-lines redistributes acetylated H2A.Z throughout the genome [73].

Extracellular Matrix Transition: ECM alterations during cardiac development and after injury, mediated by crosstalk between CMs and fibroblast sub-populations, are the subject of a recent review [82]. As shown in Figure 4, ECM genes associated with transition to soft neonatal-like matrix, which promotes CM migration and proliferation [15-17], exhibited increased expression after Tip60 KO. It is unclear why genes associated with stiffening and scarring, which encode fibrillar collagens (types 1, 3) and members of the lysyl oxidase family that regulate collagen cross-linking (*Lox*, *Loxl2*), were also up-regulated. In this regard, *Col1a1* and Lox, which is a component of soft matrix, have been associated with CM dedifferentiation [15]. It is interesting to consider that matrix softening is enhanced by the large increase in *Cthrc1* (collagen triple helix repeat containing-1), which has been shown to (i) mediate wound healing [59], (ii) limit matrix deposition during arterial remodeling [83, 84], and (iii) promote cell migration [85]. An important question regards how ECM genes, which are selectively expressed in fibroblast subpopulations [59], transition toward softness when Tip60 is depleted in CMs; although transition to soft ECM has been shown to be regulated by crosstalk between the Wnt/β-catenin, Hippo/Yap and TGFβ pathways [82], mechanistic details regarding signaling between the cells involved remains speculative.

Metabolic Reprogramming: Effects of Tip60 depletion on the expression of metabolic genes (Figs. 5-7) are consistent with multiple findings that CM dedifferentiation is accompanied by metabolic reprogramming wherein fatty acid oxidation (FAO) reverts to glycolysis (review, [86]). Most prominently, Tip60 depletion was associated with reduced expression of genes that regulate fatty acid oxidation (Fig. 5) and key steps in the TCA cycle (Fig. 6). While evidence of renewed glycolysis was not dramatic (Fig. 7a), previous observations that reversion to glycolysis during CM dedifferentiation is accompanied by increased expression of genes encoding pyruvate dehydrogenase kinase 3 (*Pdk3*), monocarboxylate transporter 3 (*Slc16a3;* Mct4) [16], and glucose transporter 1 (*Slc2a1*; Glut1) [61] were recapitulated by Tip60 depletion (Fig. 7b-c). Interestingly, although the most robustly expressed glucose transporter in CMs, *Slc2a4* (Glut4), was markedly depressed after Tip60 depletion, expression of *Slc2a1*, an isoform that is relatively weakly expressed, was upregulated (Fig. 7b-c); in this regard it may be relevant that over-expression of *Slc2a1* has been shown to mitigate heart failure [87], and was recently associated with cardiac

regeneration [88, 89]. Depletion of Tip60 after infarction was also associated with the significantly increased expression of isoforms in other glycolytic gene families (*Slc16a7*, *Pfkl*, *Eno1*, *Eno2, Ldha;* Fig. 7b-c) that are normally weakly expressed in the heart. This suggests the interesting possibility that because the dedifferentiation process reduces expression of mature isoforms that are robustly expressed in CMs, reversion to glycolysis is mediated by the increased expression of isoforms that are weakly expressed in the adult heart. To assess whether increased expression of hexokinase, along with glycolytic isoforms, is sufficient to maintain respiration in infarcted/Tip60-depleted hearts, we are conducting Seahorse assays on CMs isolated from infarcted/Tip60-depleted hearts.

Effect of Tip60 Depletion on CM Proliferation: Our previous findings that Tip60 depletion post-MI maintains cardiac function, diminishes fibrosis and activates the CM cell-cycle [10, 11], as well as the findings reported here that depletion induces a dedifferentiated state permissive for CM proliferation, are consistent with the notion that targeting Tip60 permits heart regeneration post-MI. However it remains unsettled whether bona fide proliferation of CMs ensues, expanding numbers of CMs that are mononuclear and diploid, which are considered reparative. Per our recent review [90], resolution of this seemingly straightforward question has been forestalled by the absence of a reliable method to ensure that cells positive for BrdU, Ki67 and H3P in the *in vivo* heart are indeed CMs, and are not polyploid. In future work we will address this question in depth by using a recently reported method that provides unequivocal assessment of CM identity, ploidy and nuclearity [91]. Should we find that numbers of reparative CMs are only marginally increased, methods will be deployed to further drive proliferation by exhaustively depleting Tip60.

Epigenetic Maintenance of the Differentiated State: It was recently reported that accumulation of α-ketoglutarate (αKG) resultant from CM-specific depletion of *Cpt1b* activates lysine demethylase 5 (Kdm5), reducing histone $H3K4^{me3}$ in CM 'maturity' genes to levels resulting in CM dedifferentiation and cell-cycle activation [18]. Subsequent findings by others demonstrated that systemic administration of αKG post-MI has similar effects [63]. Although Tip60 depletion did not affect the expression of *Idh2* and *Ogdh* in a fashion predicted to increase αKG levels (Fig. 6b,c), immunostaining revealed modestly reduced $H3K4^{me3}$ levels in CM nuclei (supp. Fig. 9a). Pursuant to findings that Tip60-acetylated $H2A.Zac^{K4/K7}$ and $H3K4^{me3}$ comprise a binary signature required to maintain the expression of neuronal maturity genes [64], we are utilizing CUT&Tag to assess whether depletion of Tip60 disrupts this signature in CM maturity genes.

Conclusions: These findings indicate that genetic depletion of Tip60 nearly completely extinguishes acetylation of $H2A.Zac^{K4/K7}$ in CM nuclei while inducing CM dedifferentiation. Considered with our previous findings that Tip60 depletion in CMs beginning three days post-MI promotes CM cell-cycle activation, reduces apoptosis/scarring, and preserves cardiac function [10, 11] – effects mimicked using drugs that inhibit Tip60's acetyltransferase (AT) domain [12] – pharmaceutical targeting of this pleiotropic factor is warranted to ameliorate cardiac injury. Toward this end we are developing drugs targeting Tip60's chromodomain because this moiety, which was recently shown to be required to maintain activity of Tip60's AT domain [92], is unique among the ~20 members of the MYST lysine acetyltransferase family.

Limitations of these Findings: Off-target effects of Cre-recombinase were minimized in this study by delaying determinations until 11 days after the first (of three) tamoxifen injection (i.e, 14 days post-MI), when have subsided [93]. Although Supp. Fig. 1b indicates that only ~88 genes were mis-expressed in identically treated wild-type controls expressing the *Myh6-merCremer transgene*, potential effects of Cre were observed, especially among the metabolic GO terms in Figures 5-7.

FIGURES & LEGENDS

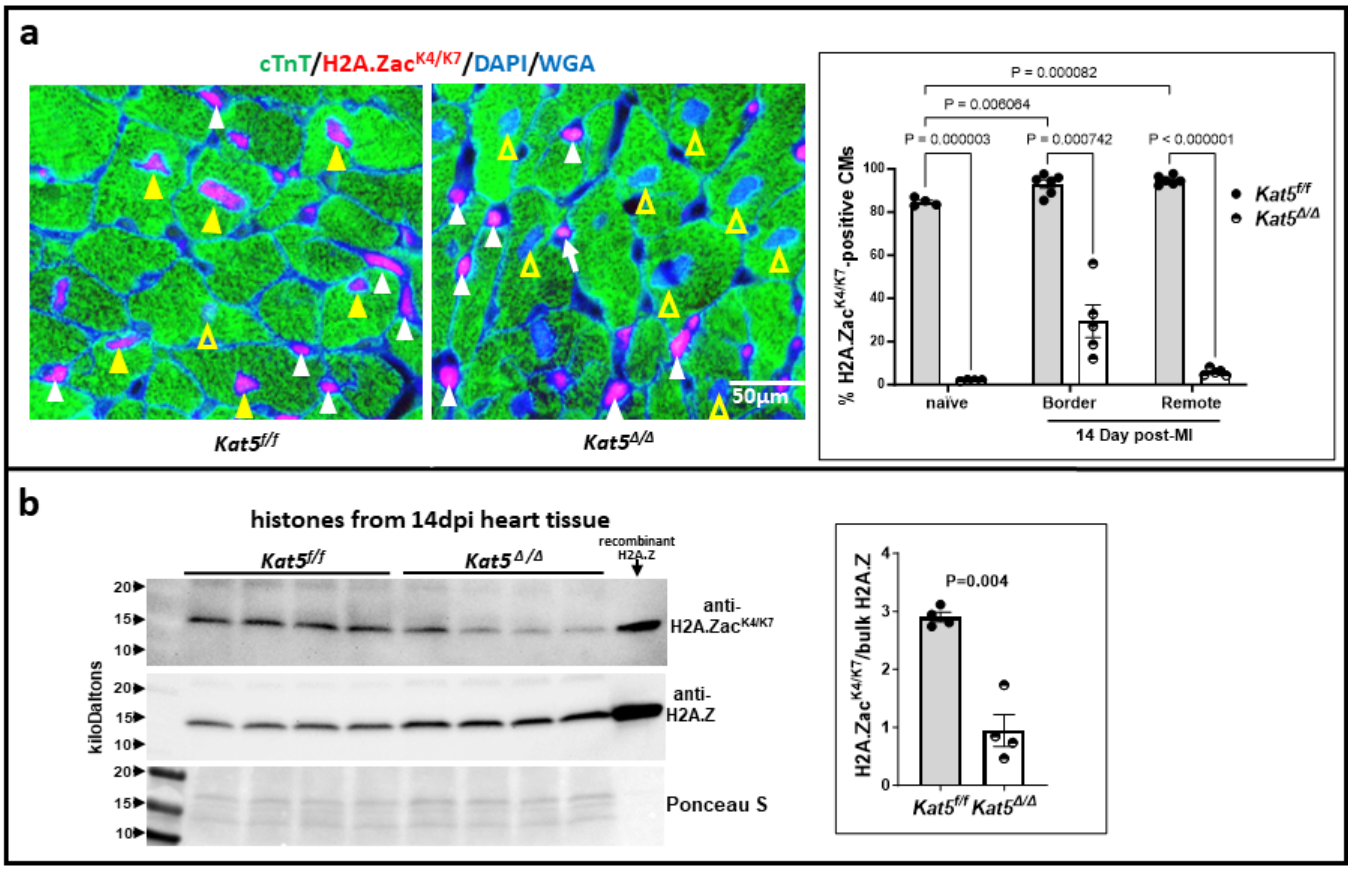

Fig. 1. Depletion of histone H2A.Z acetylation in Tip60-depleted CMs. **Panels a** & **b** respectively show representative images of control (*Kat5*$^{f/f}$) and experimental (*Kat5*$^{\Delta/\Delta}$) adult hearts wherein Tip60 was depleted from the latter by injecting tamoxifen for three consecutive days beginning on the third day after myocardial infarction (MI). Hearts were removed for processing on day 14 post-MI.

a, Immunostains: In control hearts (*Kat5*$^{f/f}$), acetylated H2A.Z (H2A.Zac; red fluorescence) is present in nuclei of most non-CMs (white arrowheads) and CMs (filled yellow arrowheads). In Tip60-depleted hearts (*Kat5*$^{\Delta/\Delta}$), H2A.Zac is present in non-CM nuclei (white arrowheads) but is conspicuously absent in most CM nuclei (open yellow arrowheads). At right, percentages of H2A.Zac-positive CMs were enumerated by blinded observers.

b, Western blots showing acetylated (above) vs. non-acetylated (i.e., bulk, middle) H2A.Z protein in heart tissue. Right, densitometry showing altered levels of H2A.Zac normalized to bulk H2A.Z.

In **panels a & b**, *P<0.05 vs. *Kat5*$^{f/f}$ per unpaired Student's t-test; means ±SEM. Each point represents a biological replicate (i.e., an individual mouse heart).

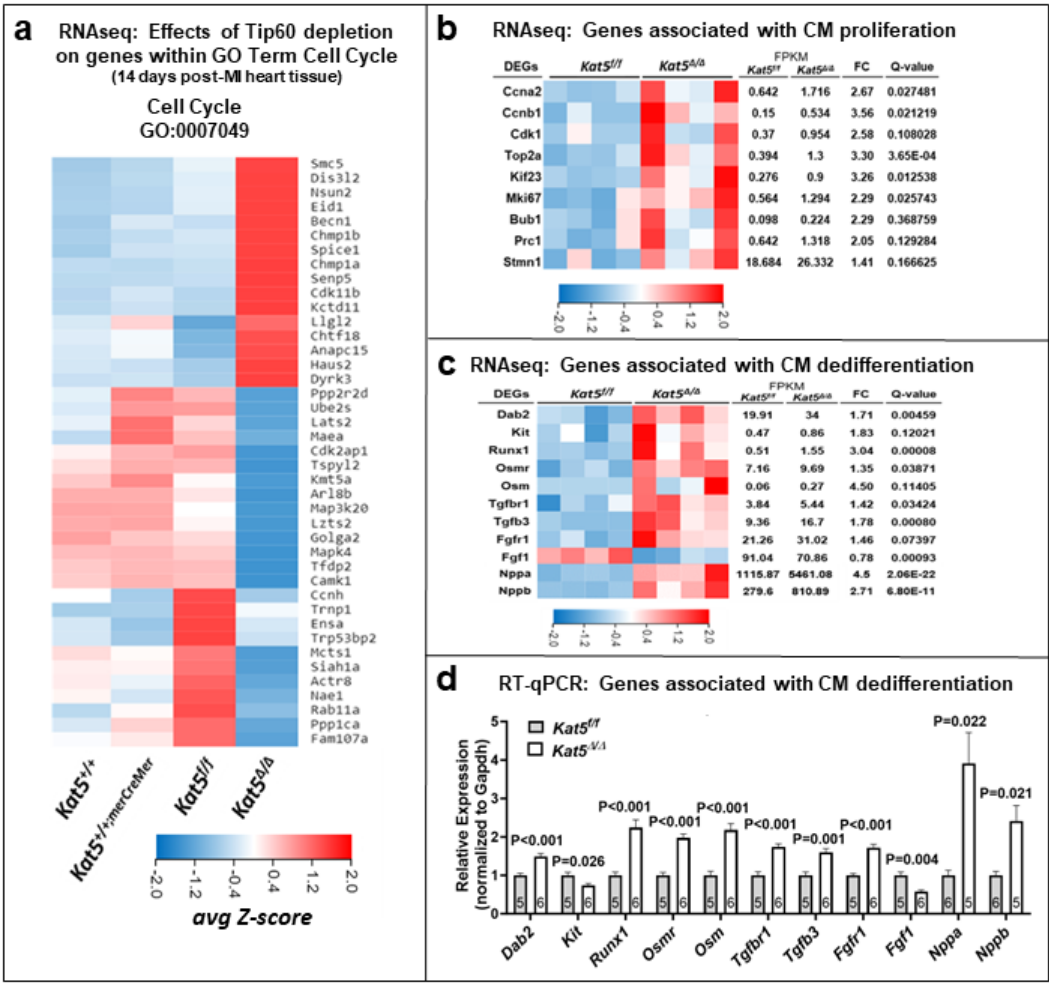

Figure 2. Expression of genes associated with pro-proliferation and de-differentiation signaling in infarcted/Tip60-depleted hearts at 14 days post-MI. Panel a: RNAseq results of Gene Ontology term Cell Cycle. **Panel b**: RNAseq data showing increased expression of pro-proliferative genes. **Panels c-d**: RNAseq (**c**) and RT-qPCR (**d**) results showing increased expression of genes associated with CM dedifferentiation. *Kat5*$^{f/f}$ = control, *Kat5*$^{\Delta/\Delta}$ = Tip60-depleted; *Kat5*$^{+/+}$ and *Kat5*$^{+/+;merCremer}$ were controls to assess off-target effects of Cre-recombinase. In **b-c** each column represents a biological replicate. In **d**, each biological replicate (N, inside bar) is a single heart, each subjected to three technical replicates. Data are Mean ±SEM, compared by unpaired, two-tailed Student's t tests with Welch's correction.

Figure 3

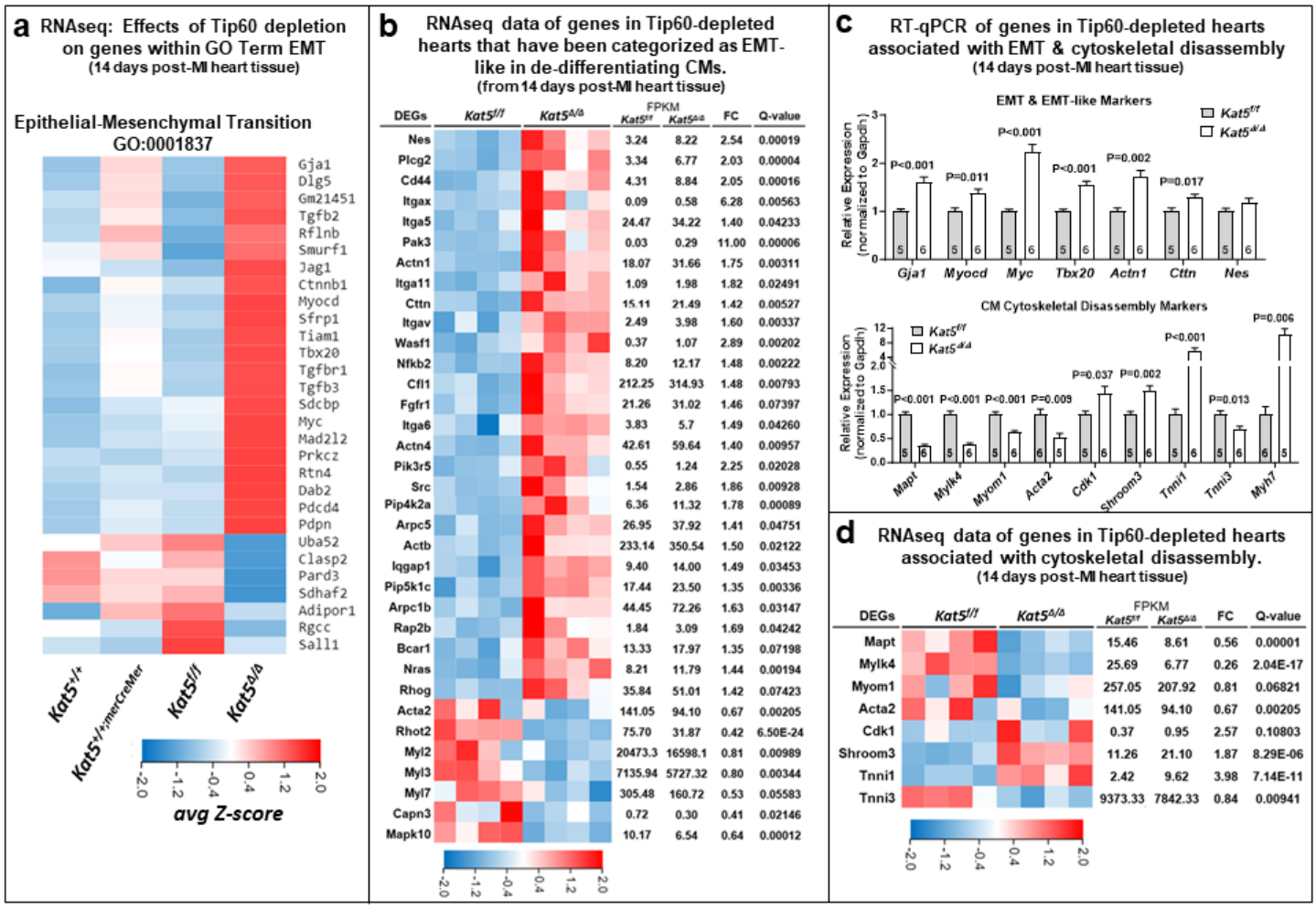

Figure 3. Expression of genes associated with epithelial-mesenchymal transition (EMT) & cytoskeleton stability in infarcted/Tip60-depleted hearts. Panel a, RNAseq: effect on genes in the Gene Ontology term Epithelial Mesenchymal Transition (EMT). **Panel b, RNAseq:** mis-expressed EMT-like genes. **Panel c, RT-qPCR:** mis-expressed EMT, EMT-like and cytoskeletal genes. **Panel d, RNAseq:** mis-expressed cytoskeletal genes. *Kat5*$^{f/f}$ = control, *Kat5*$^{\Delta/\Delta}$ = Tip60-depleted. In **a**, *Kat5*$^{+/+}$ vs. *Kat5*$^{+/+;merCremer}$ assess off-target effects of Cre-recombinase. In **b**, each column represents a biological replicate. In **c**, each biological replicate (N inside bars) is a single heart, each subjected to three technical replicates. RT-qPCR data are Mean ±SEM compared by unpaired two-tailed Student's t tests with Welch's correction.

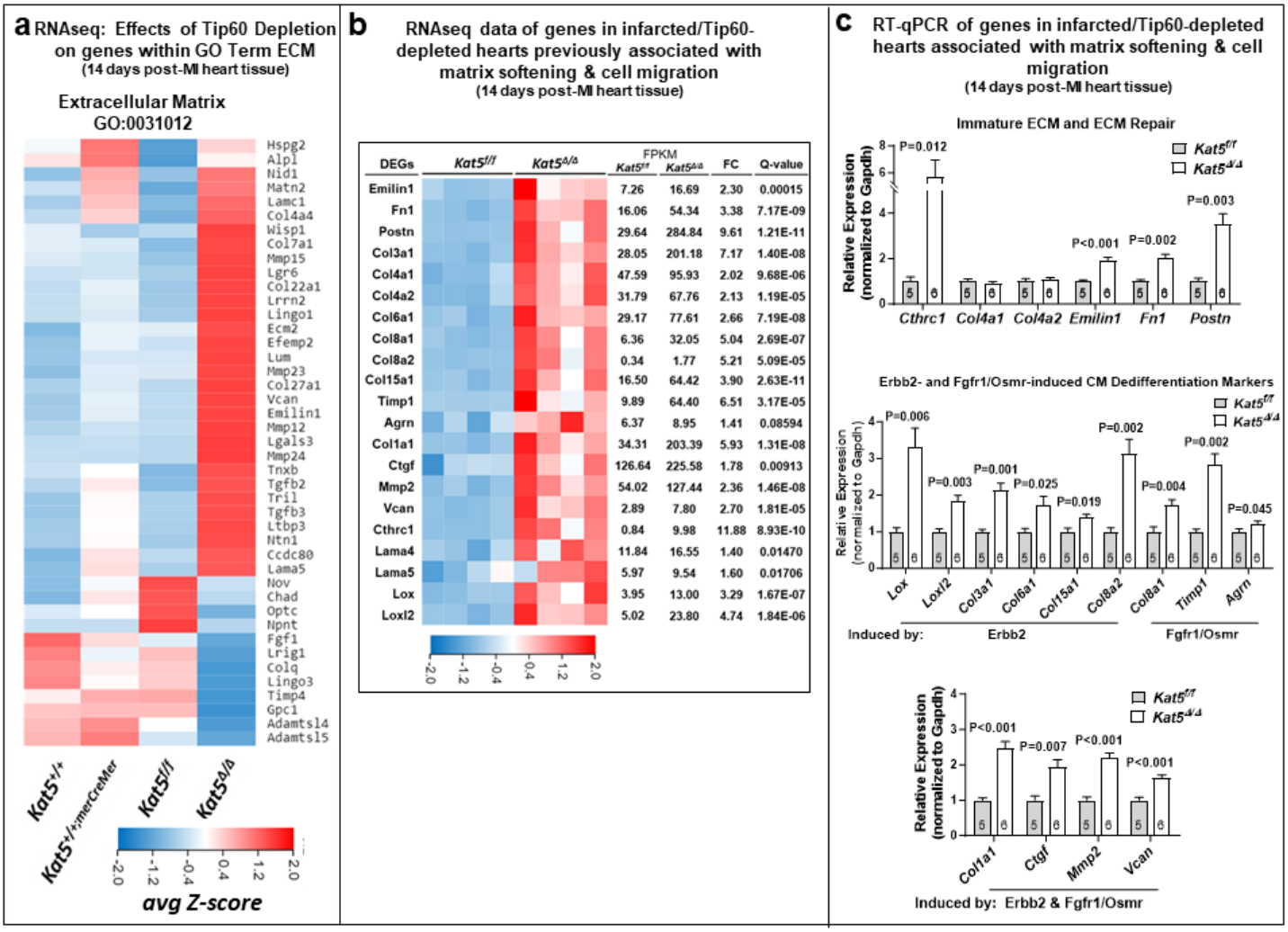

Figure 4. Increased expression of genes associated with transition to soft connective tissue and cell migration in infarcted/Tip60-depleted hearts at 14 days post-infarction. Panel a, RNAseq: Up- and down-regulated genes in the GO term Extracellular Matrix (ECM). **Panel b, RNAseq:** Increased expression of ECM genes in infarcted/Tip60-depleted hearts. **Panel c, RT-qPCR**: ECM genes exhibiting increased expression in Tip60-depleted hearts, including genes shown by others to be increased by over-expressing Erbb2 or inducing Fgfr1/OsmR. *Kat5*$^{f/f}$ = control, *Kat5*$^{\Delta/\Delta}$ = Tip60-depleted. In **a**, *Kat5*$^{+/+}$ and *Kat5*$^{+/+;merCremer}$ are controls to assess off-target effects of Cre-recombinase. In **b**, each column represents a biological replicate. In **c**, each biological replicate (N inside bars) is a single heart, each subjected to three technical replicates. Data are Mean ±SEM, compared by unpaired, two-tailed Student's t tests with Welch's correction.

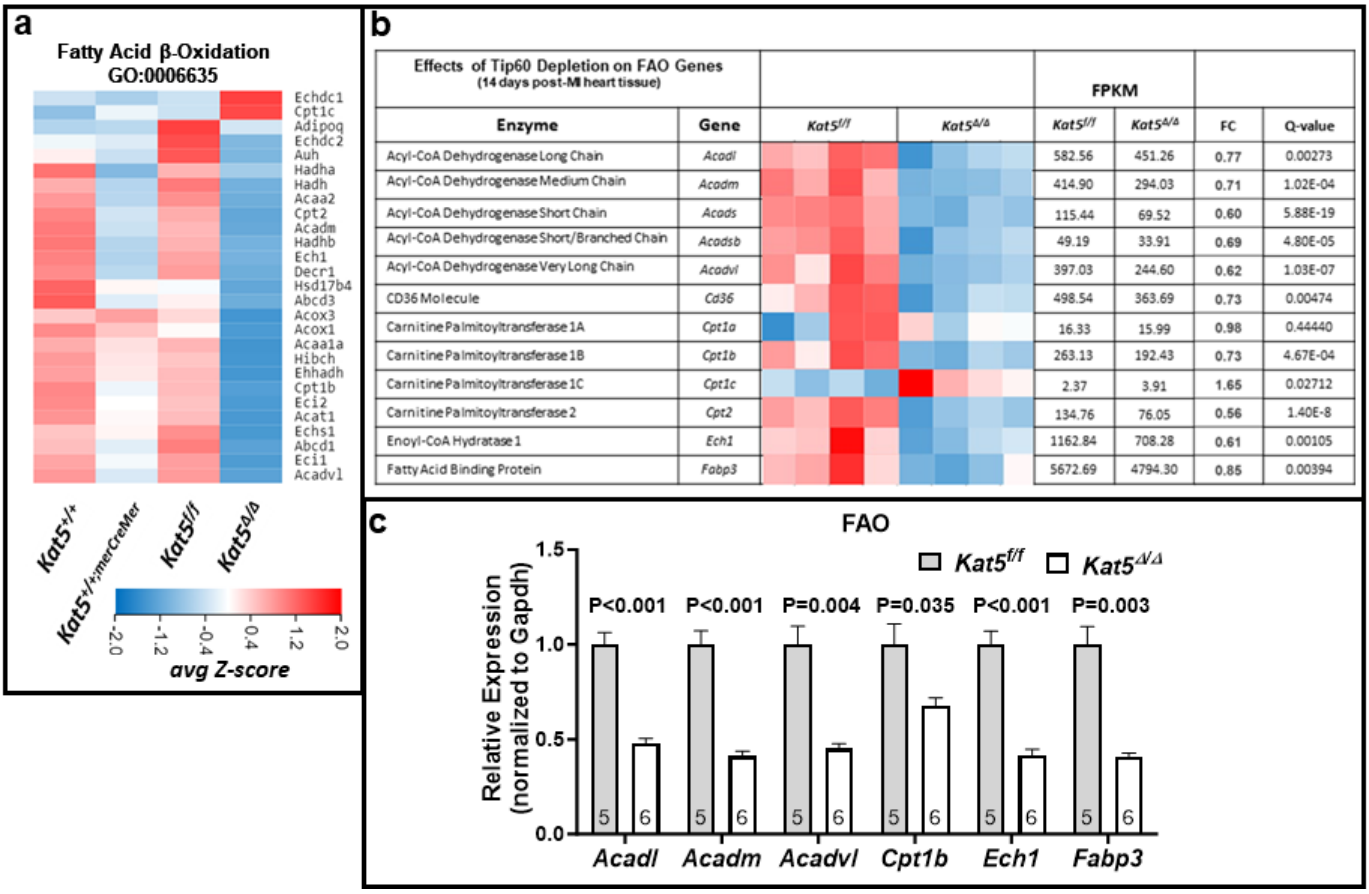

Effects of Tip60 Depletion on FAO Genes (14 days post-MI heart tissue)				FPKM			
Enzyme	Gene	*Kat5*$^{f/f}$	*Kat5*$^{\Delta/\Delta}$	*Kat5*$^{f/f}$	*Kat5*$^{\Delta/\Delta}$	FC	Q-value
Acyl-CoA Dehydrogenase Long Chain	*Acadl*			582.56	451.26	0.77	0.00273
Acyl-CoA Dehydrogenase Medium Chain	*Acadm*			414.90	294.03	0.71	1.02E-04
Acyl-CoA Dehydrogenase Short Chain	*Acads*			115.44	69.52	0.60	5.88E-19
Acyl-CoA Dehydrogenase Short/Branched Chain	*Acadsb*			49.19	33.91	0.69	4.80E-05
Acyl-CoA Dehydrogenase Very Long Chain	*Acadvl*			397.03	244.60	0.62	1.03E-07
CD36 Molecule	*Cd36*			498.54	363.69	0.73	0.00474
Carnitine Palmitoyltransferase 1A	*Cpt1a*			16.33	15.99	0.98	0.44440
Carnitine Palmitoyltransferase 1B	*Cpt1b*			263.13	192.43	0.73	4.67E-04
Carnitine Palmitoyltransferase 1C	*Cpt1c*			2.37	3.91	1.65	0.02712
Carnitine Palmitoyltransferase 2	*Cpt2*			134.76	76.05	0.56	1.40E-8
Enoyl-CoA Hydratase 1	*Ech1*			1162.84	708.28	0.61	0.00105
Fatty Acid Binding Protein	*Fabp3*			5672.69	4794.30	0.85	0.00394

Figure 5. Expression of genes associated with fatty acid oxidation in infarcted/Tip60-depleted hearts at 14 days post-infarction. Panel a: RNAseq results showing gene mis-expressions in the GO term Fatty Acid β-Oxidation (FAO). *Kat5*$^{f/f}$ = control, *Kat5*$^{\Delta/\Delta}$ = Tip60-depleted. *Kat5*$^{+/+}$ and *Kat5*$^{+/+;merCremer}$ were compared to assess off-target effects of Cre-recombinase. **Panel b:** RNAseq data of mis-expressed key FAO enzymes in infarcted/Tip60-depleted hearts at 14 days post-MI. Each colored column represents a biological replicate. **Panel c:** RT-qPCR data showing mis-expression of selected genes that regulate FAO in infarcted/Tip60-depleted hearts. Each biological replicate (N; shown inside bar) is from a single heart; each was subjected to three technical replicates. Data are Mean ± SEM, compared by unpaired, two-tailed Student's t tests with Welch's correction.

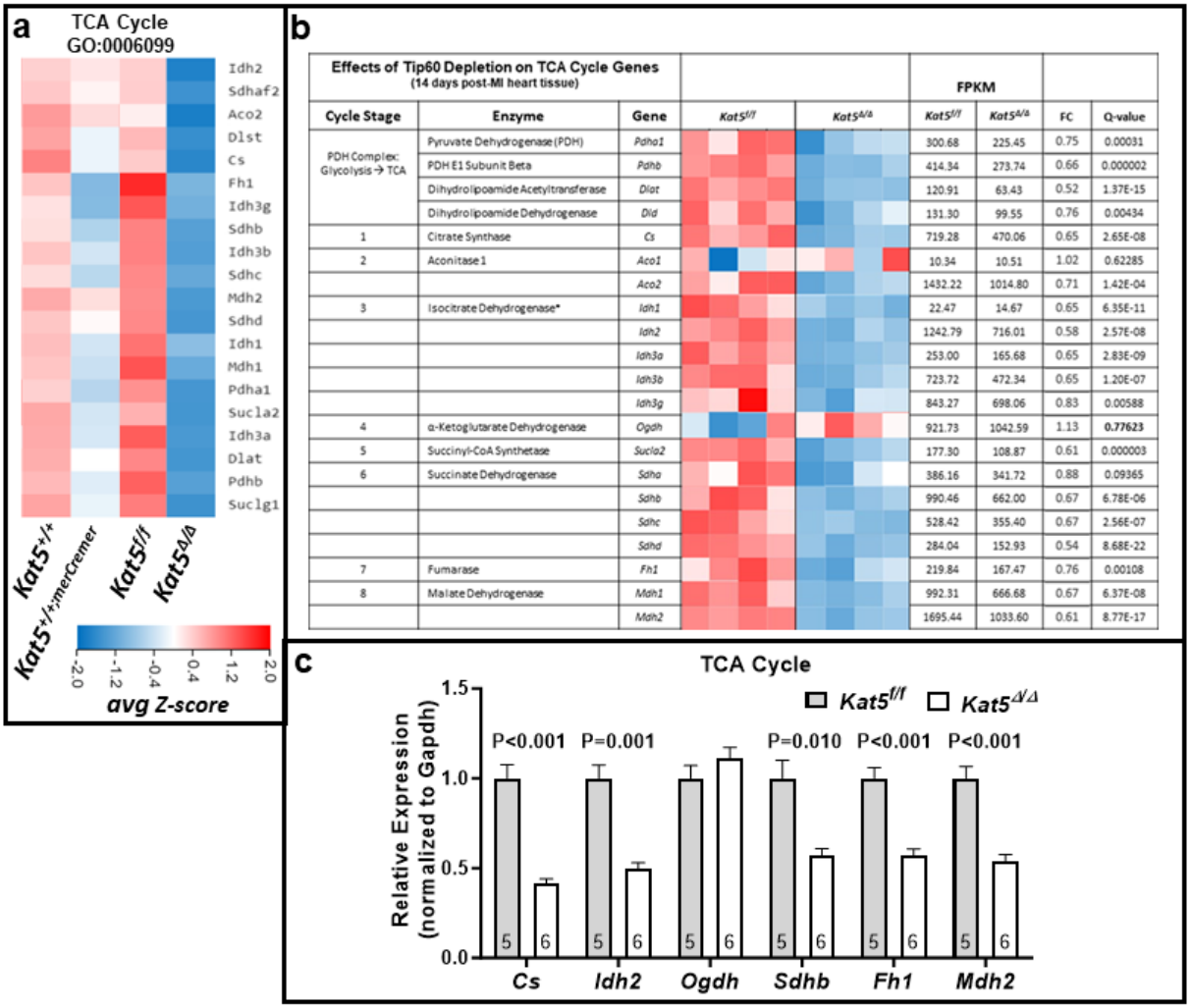

Effects of Tip60 Depletion on TCA Cycle Genes (14 days post-MI heart tissue)

Cycle Stage	Enzyme	Gene	*Kat5*$^{f/f}$	*Kat5*$^{\Delta/\Delta}$	FPKM *Kat5*$^{f/f}$	FPKM *Kat5*$^{\Delta/\Delta}$	FC	Q-value
PDH Complex: Glycolysis → TCA	Pyruvate Dehydrogenase (PDH)	*Pdha1*			300.68	225.45	0.75	0.00031
	PDH E1 Subunit Beta	*Pdhb*			414.34	273.74	0.66	0.000002
	Dihydrolipoamide Acetyltransferase	*Dlat*			120.91	63.43	0.52	1.37E-15
	Dihydrolipoamide Dehydrogenase	*Dld*			131.30	99.55	0.76	0.00434
1	Citrate Synthase	*Cs*			719.28	470.06	0.65	2.65E-08
2	Aconitase 1	*Aco1*			10.34	10.51	1.02	0.62285
		Aco2			1432.22	1014.80	0.71	1.42E-04
3	Isocitrate Dehydrogenase*	*Idh1*			22.47	14.67	0.65	6.35E-11
		Idh2			1242.79	716.01	0.58	2.57E-08
		Idh3a			253.00	165.68	0.65	2.83E-09
		Idh3b			723.72	472.34	0.65	1.20E-07
		Idh3g			843.27	698.06	0.83	0.00588
4	α-Ketoglutarate Dehydrogenase	*Ogdh*			921.73	1042.59	1.13	**0.77623**
5	Succinyl-CoA Synthetase	*Sucla2*			177.30	108.87	0.61	0.000003
6	Succinate Dehydrogenase	*Sdha*			386.16	341.72	0.88	0.09365
		Sdhb			990.46	662.00	0.67	6.78E-06
		Sdhc			528.42	355.40	0.67	2.56E-07
		Sdhd			284.04	152.93	0.54	8.68E-22
7	Fumarase	*Fh1*			219.84	167.47	0.76	0.00108
8	Malate Dehydrogenase	*Mdh1*			992.31	666.68	0.67	6.37E-08
		Mdh2			1695.44	1033.60	0.61	8.77E-17

Figure 6. Expression of genes associated with TCA cycle in infarcted/Tip60-depleted hearts at 14 days post-infarction. Panel a: RNAseq results showing gene mis-expressions in the GO term TCA cycle. *Kat5*$^{f/f}$ = control, *Kat5*$^{\Delta/\Delta}$ = Tip60-depleted. *Kat5*$^{+/+}$ and *Kat5*$^{+/+;merCremer}$ were compared to assess off-target effects of Cre-recombinase. **Panel b:** RNAseq data of mis-expressed enzymes that regulate each TCA cycle stage in infarcted/Tip60-depleted hearts at 14 days post-MI. Each colored column represents a biological replicate. **Panel c:** RT-qPCR data showing mis-expression of TCA cycle genes in infarcted/Tip60-depleted hearts. Each biological replicate (N; shown inside bar) is from a single heart; each was subjected to three technical replicates. Data are Mean ± SEM, compared by unpaired, two-tailed Student's t tests with Welch's correction.

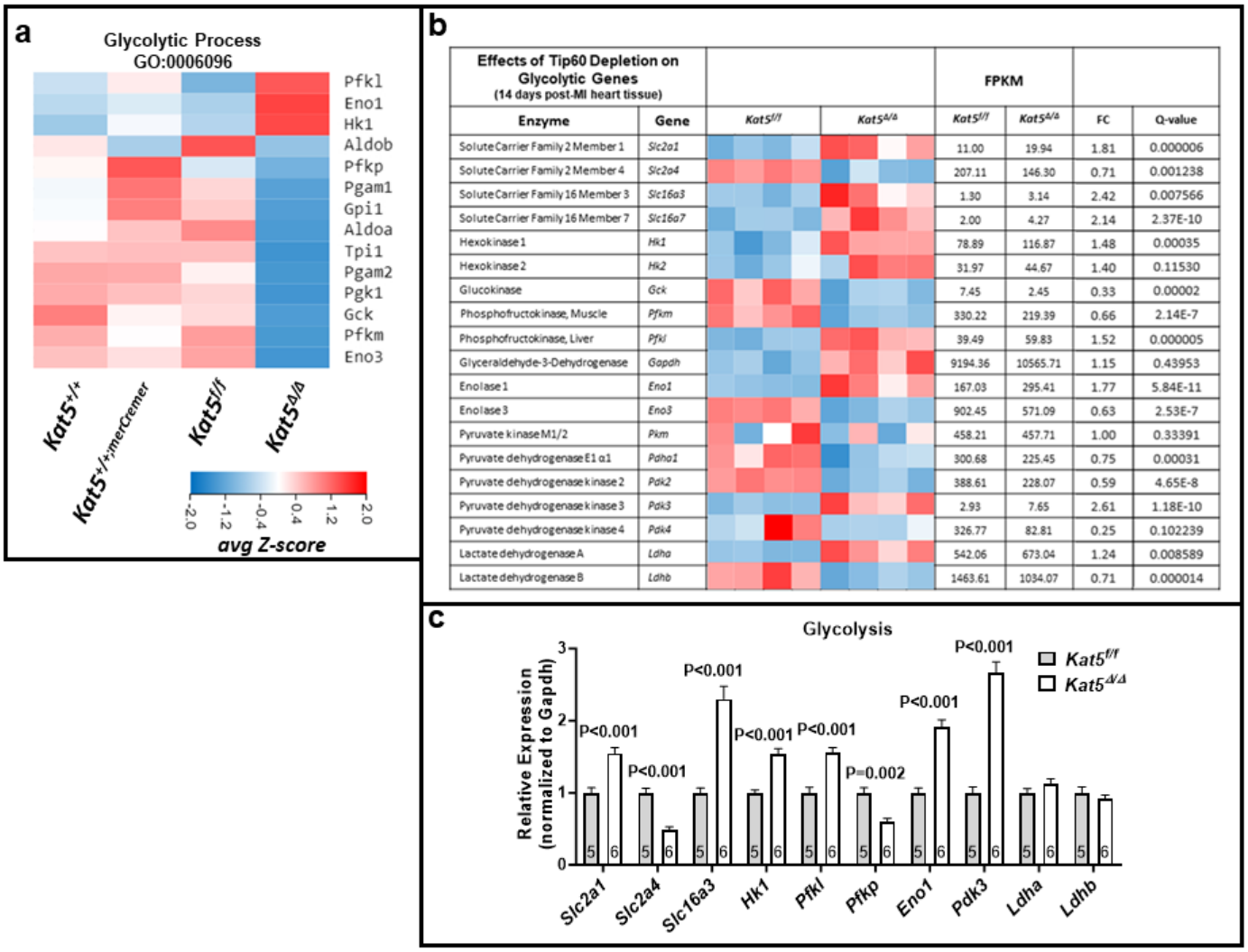

Effects of Tip60 Depletion on Glycolytic Genes (14 days post-MI heart tissue)

Enzyme	Gene	*Kat5f/f*	*Kat5Δ/Δ*	FPKM *Kat5f/f*	FPKM *Kat5Δ/Δ*	FC	Q-value
Solute Carrier Family 2 Member 1	*Slc2a1*			11.00	19.94	1.81	0.000006
Solute Carrier Family 2 Member 4	*Slc2a4*			207.11	146.30	0.71	0.001238
Solute Carrier Family 16 Member 3	*Slc16a3*			1.30	3.14	2.42	0.007566
Solute Carrier Family 16 Member 7	*Slc16a7*			2.00	4.27	2.14	2.37E-10
Hexokinase 1	*Hk1*			78.89	116.87	1.48	0.00035
Hexokinase 2	*Hk2*			31.97	44.67	1.40	0.11530
Glucokinase	*Gck*			7.45	2.45	0.33	0.00002
Phosphofructokinase, Muscle	*Pfkm*			330.22	219.39	0.66	2.14E-7
Phosphofructokinase, Liver	*Pfkl*			39.49	59.83	1.52	0.000005
Glyceraldehyde-3-Dehydrogenase	*Gapdh*			9194.36	10565.71	1.15	0.43953
Enolase 1	*Eno1*			167.03	295.41	1.77	5.84E-11
Enolase 3	*Eno3*			902.45	571.09	0.63	2.53E-7
Pyruvate kinase M1/2	*Pkm*			458.21	457.71	1.00	0.33391
Pyruvate dehydrogenase E1 α1	*Pdha1*			300.68	225.45	0.75	0.00031
Pyruvate dehydrogenase kinase 2	*Pdk2*			388.61	228.07	0.59	4.65E-8
Pyruvate dehydrogenase kinase 3	*Pdk3*			2.93	7.65	2.61	1.18E-10
Pyruvate dehydrogenase kinase 4	*Pdk4*			326.77	82.81	0.25	0.102239
Lactate dehydrogenase A	*Ldha*			542.06	673.04	1.24	0.008589
Lactate dehydrogenase B	*Ldhb*			1463.61	1034.07	0.71	0.000014

Figure 7. Expression of glycolysis-associated genes in infarcted/Tip60-depleted hearts at 14 days post-infarction. Panel a: RNAseq results showing gene mis-expressions in the GO term Glycolytic Process. *Kat5*$^{f/f}$ = control, *Kat5*$^{\Delta/\Delta}$ = Tip60-depleted. *Kat5*$^{+/+}$ and *Kat5*$^{+/+;merCremer}$ were compared to assess off-target effects of Cre-recombinase. **Panel b:** RNAseq data of mis-expressed genes that regulate glycolytic steps in infarcted/Tip60-depleted hearts at 14 days post-MI. Each colored column represents a biological replicate. **Panel c:** RT-qPCR data showing altered expression of the glycolytic process gene isoforms in infarcted/Tip60-depleted hearts. Each biological replicate (N; shown inside bar) is from a single heart; each was subjected to three technical replicates. Data are Mean ± SEM, compared by unpaired, two-tailed Student's t tests with Welch's correction.

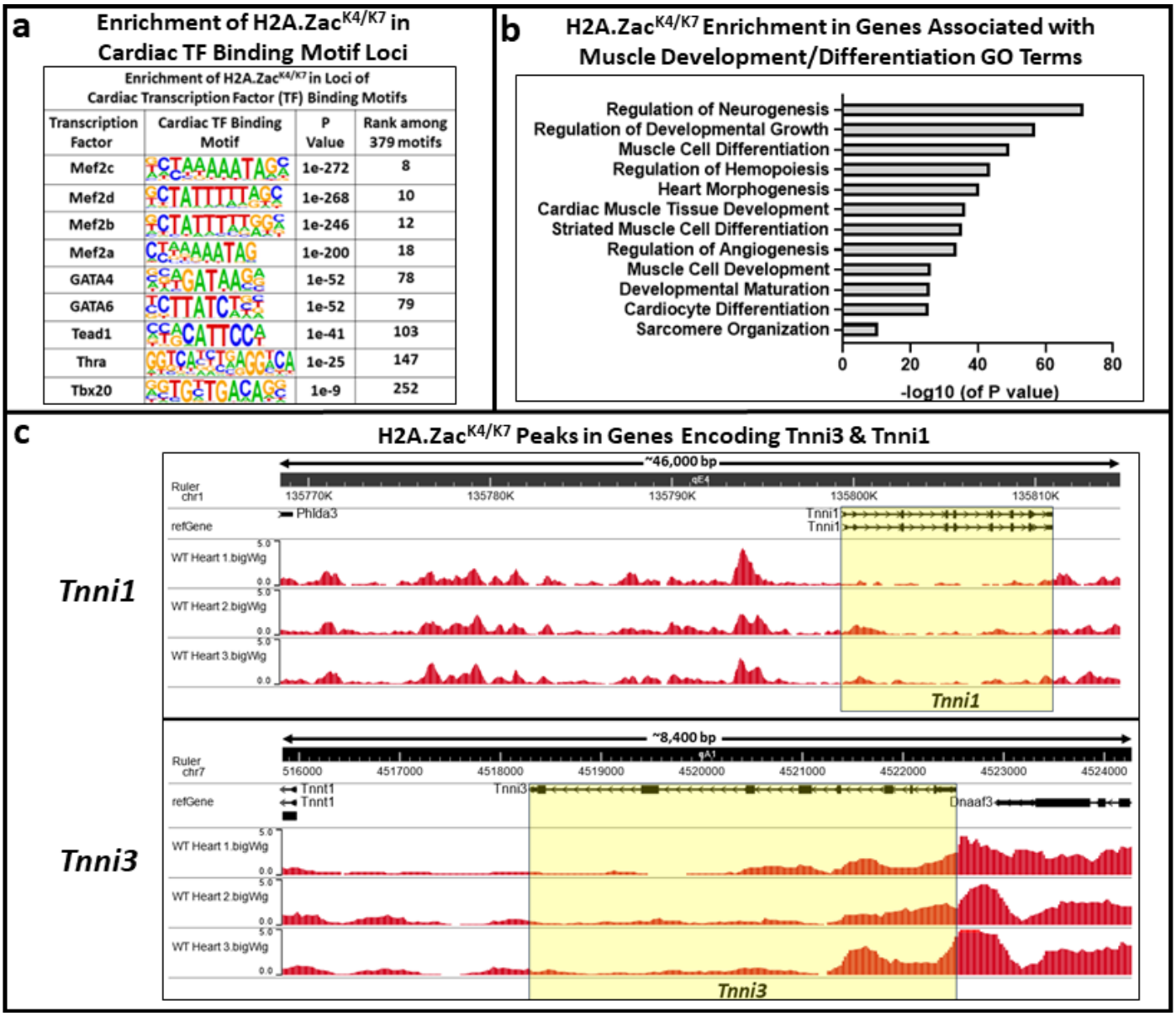

Figure 8. H2A.Zac$^{K4/K7}$ peaks in transcription factor (TF) motifs and genes associated with cardiomyocyte differentiation identified using CUT&Tag. Panel a: Cardiac TF binding motifs enriched in H2A.Zac$^{K4/K7}$, identified using Homer (Hypergeometric Optimization of Motif EnRichment). **Panel b**: Gene ontology (GO) terms involving muscle cell differentiation and development associated with H2A.Zac$^{K4/K7}$ peaks**. Panel c:** WashU genome browser tracks showing H2A.Zac$^{K4/K7}$ peaks in genes encoding Tnni1 (upper) and Tnni3 (lower). Data in all panels was derived from CUT&Tag determinations on nuclei isolated from left ventricles of three wild-type adult hearts, which were neither infarcted nor treated with tamoxifen.

SUPPLEMENTAL FIGURES & LEGENDS

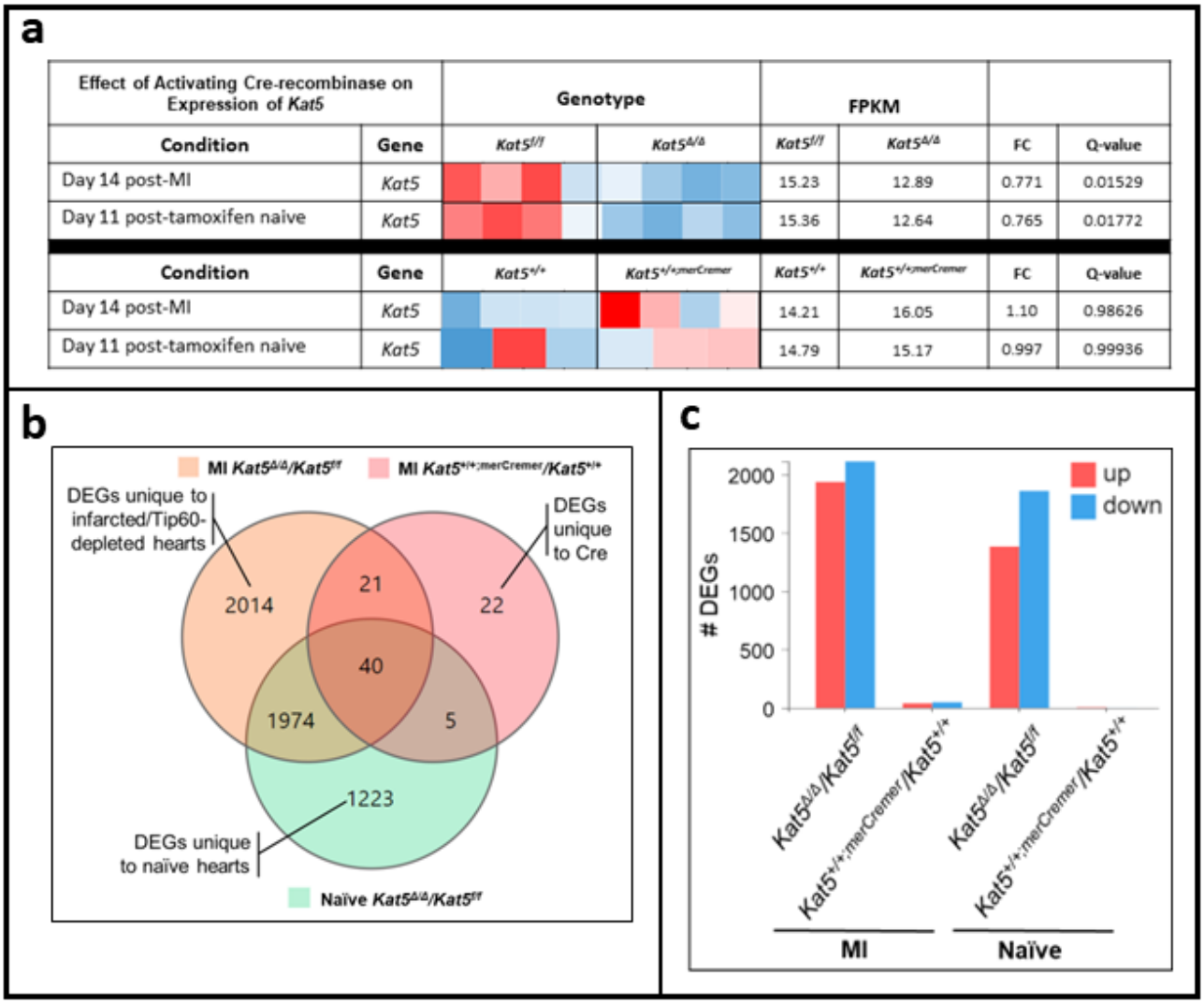

Effect of Activating Cre-recombinase on Expression of *Kat5*		Genotype		FPKM			
Condition	**Gene**	*Kat5*$^{f/f}$	*Kat5*$^{\Delta/\Delta}$	*Kat5*$^{f/f}$	*Kat5*$^{\Delta/\Delta}$	**FC**	**Q-value**
Day 14 post-MI	*Kat5*			15.23	12.89	0.771	0.01529
Day 11 post-tamoxifen naive	*Kat5*			15.36	12.64	0.765	0.01772
Condition	**Gene**	*Kat5*$^{+/+}$	*Kat5*$^{+/+;merCremer}$	*Kat5*$^{+/+}$	*Kat5*$^{+/+;merCremer}$	**FC**	**Q-value**
Day 14 post-MI	*Kat5*			14.21	16.05	1.10	0.98626
Day 11 post-tamoxifen naive	*Kat5*			14.79	15.17	0.997	0.99936

Supplemental Figure 1. Effects of Tip60 depletion on gene expression in infarcted and naïve hearts. Panel a: RNAseq results showing the extent of Tip60 depletion. Twelve-week-old *Kat5*$^{f/f}$, *Kat5*$^{\Delta/\Delta}$, *Kat5*$^{+/+}$, and *Kat5*$^{+/+;merCremer}$ mice were infarcted (see Methods). Beginning on the third day after myocardial infarction (MI), mice were intraperitoneally injected with 40 mg/kg tamoxifen for three consecutive days. On the 14th day post-MI, hearts were collected and processed for total RNA. Naïve mice of similar age were intraperitoneally injected with 40 mg/kg tamoxifen for three consecutive days and hearts were collected and processed for RNA on the 11 day after the first injection. Each colored column represents a biological replicate. **Panel b:** Venn diagram depicting overlap of differentially expressed genes (DEGs) between different comparison groups. **Panel c:** Total number of up/down-regulated DEGs in naïve and infarcted hearts. Minimal off-target effects of Cre-recombinase were observed comparing *Kat5*$^{+/+}$ vs. *Kat5*$^{+/+;merCremer}$.

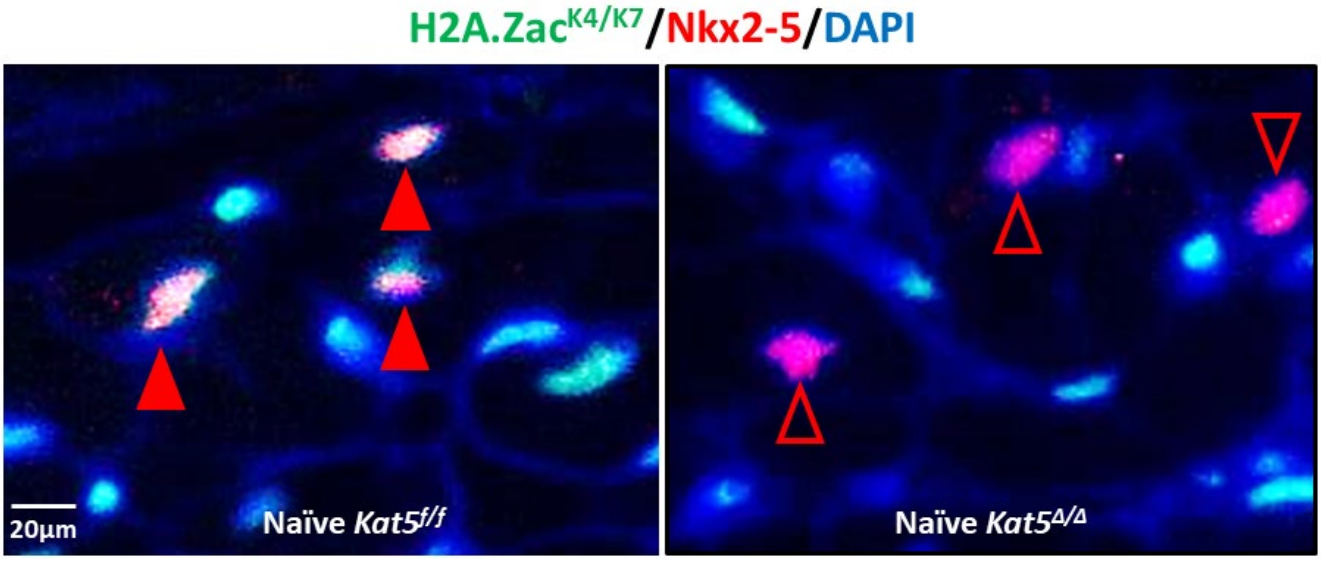

Supplemental Figure 2. Verification of cardiomyocyte identity by immunostaining Nkx2-5. Closed red arrowheads in naïve control (*Kat5*$^{f/f}$) myocardium denote CM nuclei containing acetylated H2A.Z (H2A.Zac$^{K4/K7}$). Open red arrowheads in naïve myocardium after Tip60 depletion (*Kat5*$^{Δ/Δ}$) denote CM nuclei devoid of acetylated H2A.Z. Red fluorescent staining identifies Nkx2-5.

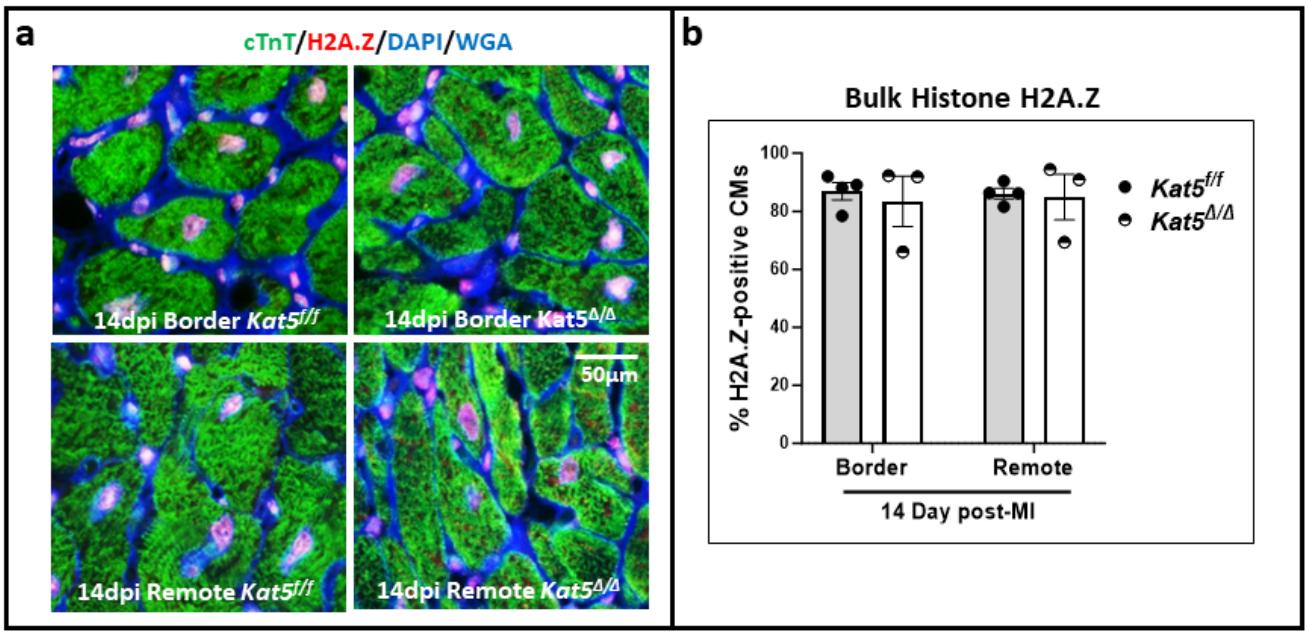

Supplemental Figure 3. Numbers of CMs containing bulk histone H2A.Z in infarcted hearts are unaffected by Tip60 depletion. Panel a, immunostaining bulk histone H2A.Z in CMs using anti-H2A.Z); CMs were identified using anti-cardiac troponin-T antibody. **Panel b**, total numbers of CMs and total numbers of H2A.Z-positive CMs were separately assessed at 400x magnification in six cross-sectional fields each within the border and remote zones; percentages of H2A.Z-positive CMs in each field were then averaged to obtain the percentages shown. *P<0.05 vs. *Kat5*$^{f/f}$ per unpaired Student's t-test; means ±SEM.

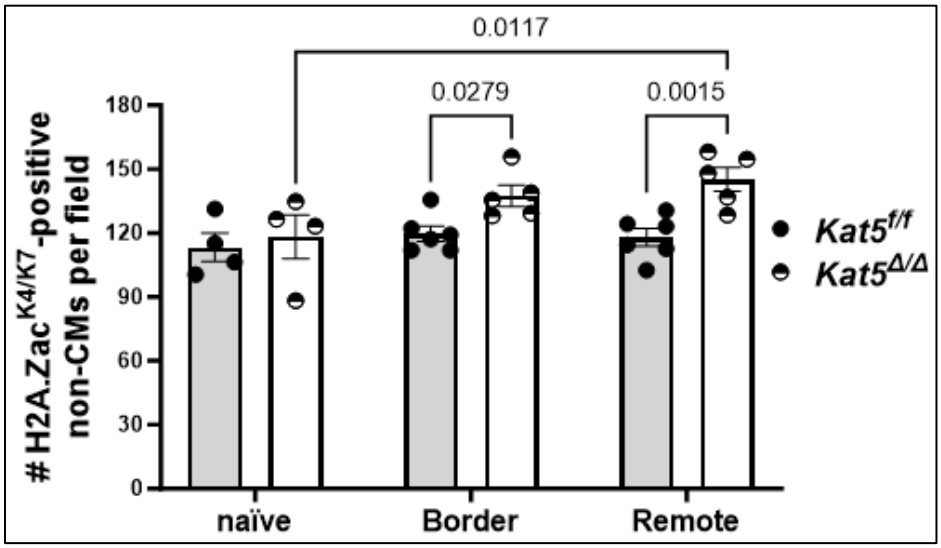

Supplemental Figure 4. H2A.Zac$^{K4/K7}$-positive interstitial cells (i.e., non-CMs) in naïve and infarcted Tip60-depleted hearts. P values calculated by two-way ANOVA with Bonferroni's multiple comparisons; means ±SEM.

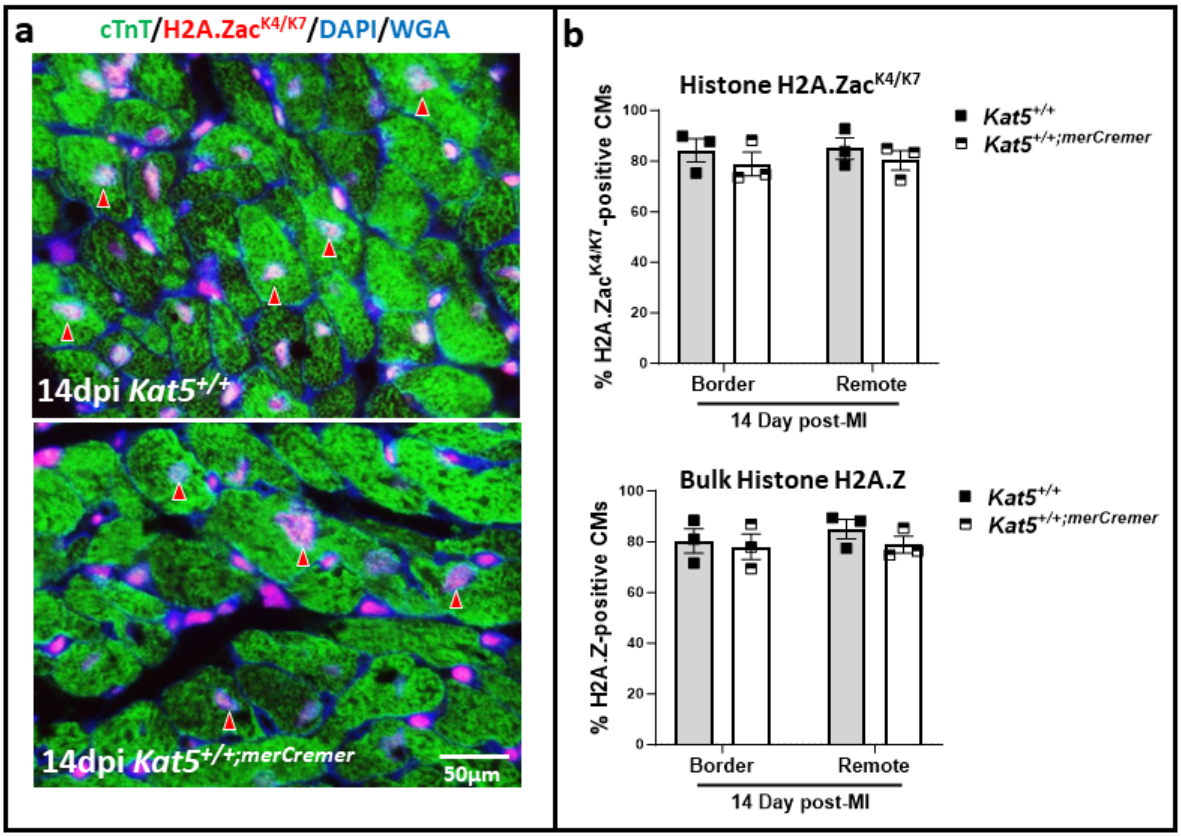

Supplemental Figure 5. Cre recombinase, alone, does not affect numbers of CMs containing H2A.Zac$^{K4/K7}$ or bulk histone H2A.Z in infarcted hearts. Panel a, typical immunostains showing H2A.Zac$^{K4/K7}$-positive (red fluorescence) nuclei in wild-type CMs (*Kat5*$^{+/+}$, above) and in CMs expressing tamoxifen-activated Cre-recombinase (*Kat5*$^{+/+;merCremer}$, below). Red arrowheads denote H2A.Zac$^{K4/K7}$-positive CMs. **Panel b** shows enumeration of H2A.Zac$^{K4/K7}$-positive CMs (above), as well as CMs enumerated for content of bulk histone H2A.Z (below). In both instances CMs were identified by immunostaining with anti-cardiac troponin-T (green fluorescence) combined with WGA. *P<0.05 vs. *Kat5*$^{+/+}$ per unpaired Student's t-test; means ±SEM.

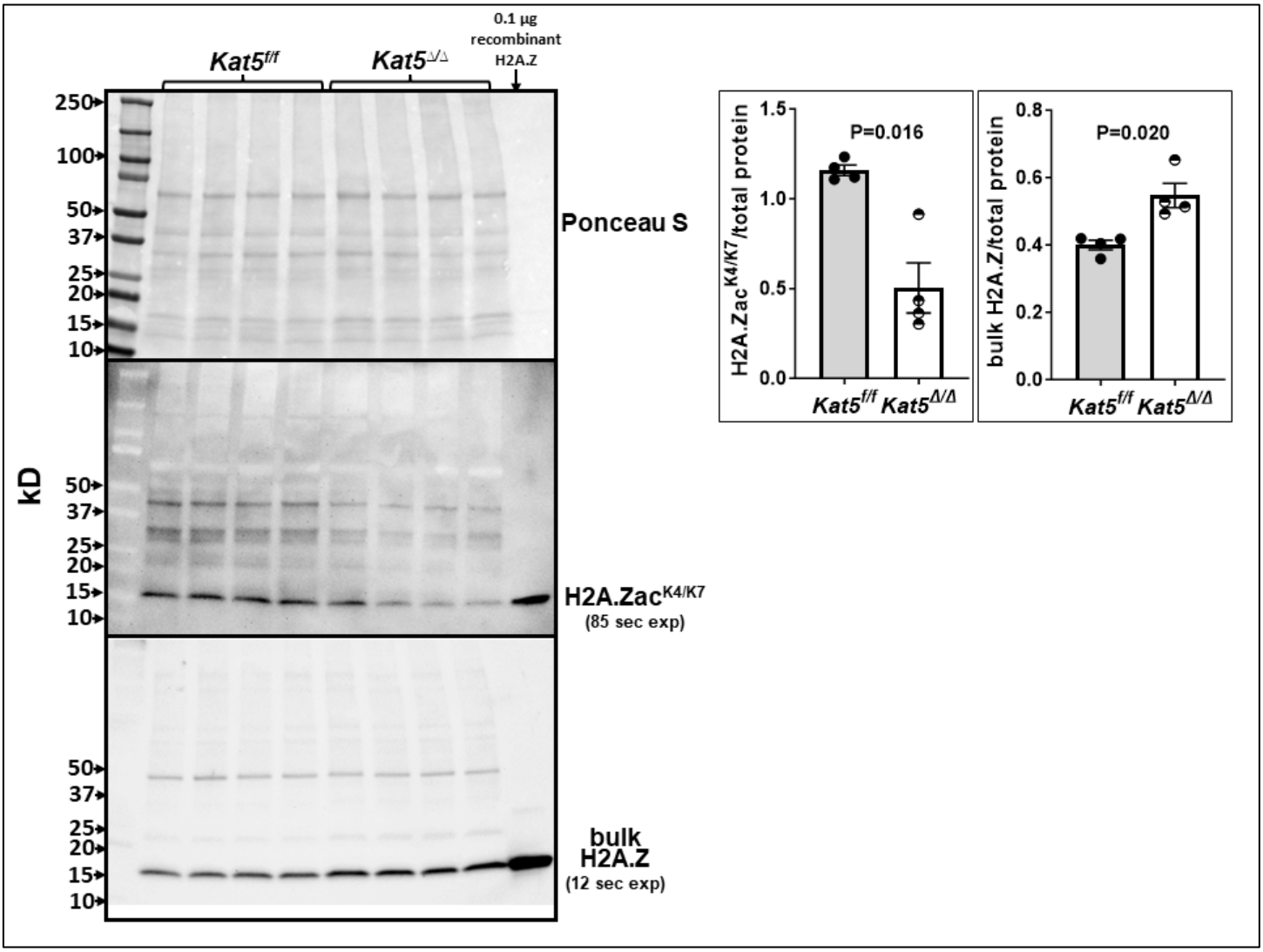

Supplemental Figure 6. Non-cropped western blots showing reduced levels of acetylated H2A.Zac$^{K4/K7}$ in Tip60-depleted (*Kat5*$^{\Delta/\Delta}$) hearts. Each point represents a biological replicate (i.e., an individual mouse heart). According to the manufacturer (Cell Signaling Technology) of the anti-H2A.Zac$^{K4/K7}$ antibody, the ~22 kDa band represents mono-ubiquitinated H2A.Z.

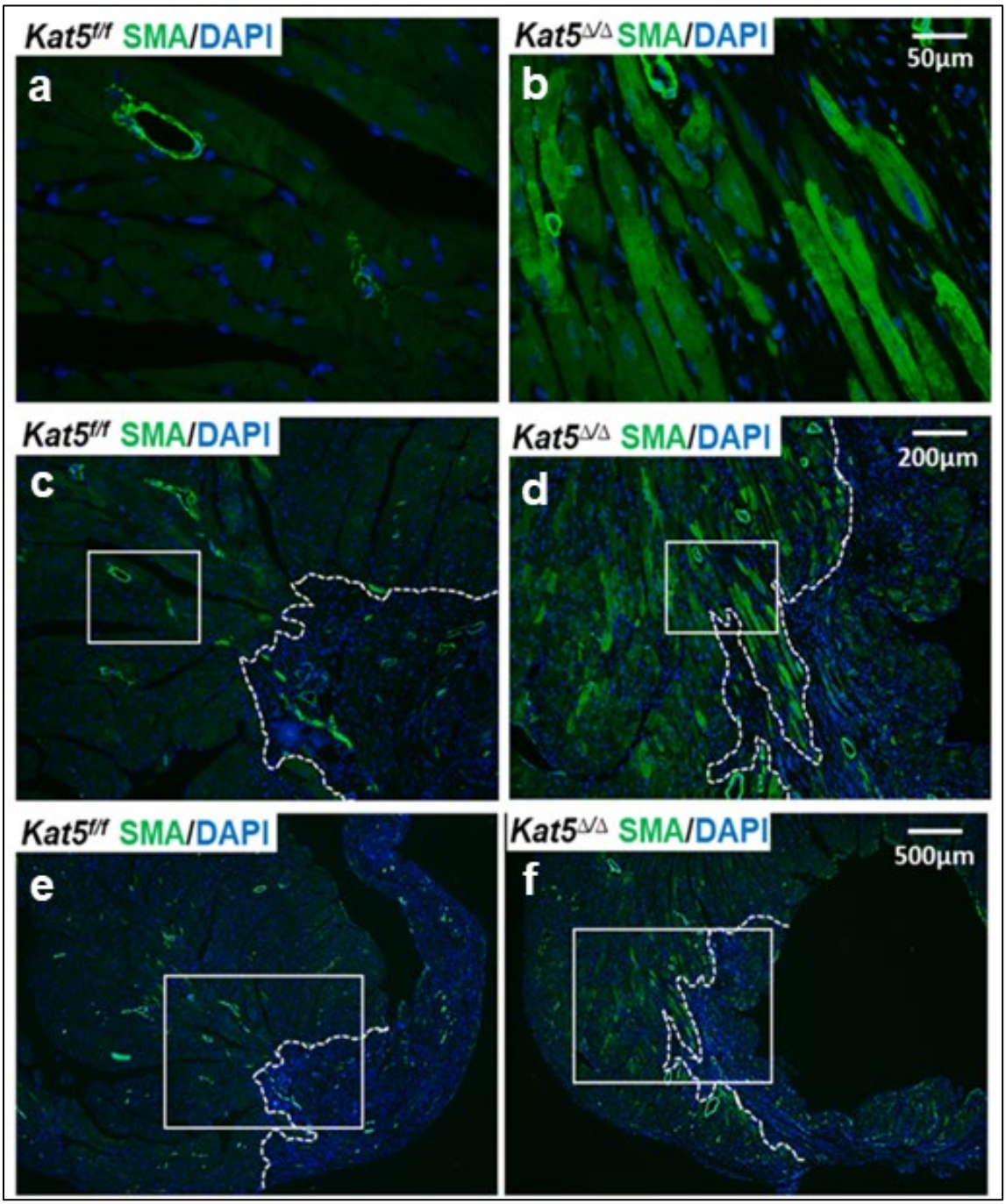

Supplemental Figure 7. Immunostains showing up-regulation of α-smooth muscle actin (α-SMA) in CMs within the border zone of infarcted/Tip60-depleted hearts. Panels a-f are representative images of control ($Kat5^{f/f}$) and Tip60-depleted ($Kat5^{\Delta/\Delta}$) hearts at 28 days post-MI. Striated, α-SMA-positive CMs are aligned along the border zone of Tip60-depleted hearts. **Panels a-b** are shown at reduced magnifications in the white rectangles in panels c-f. The broken white line in panels c-f demarcates the border and infarct zones.

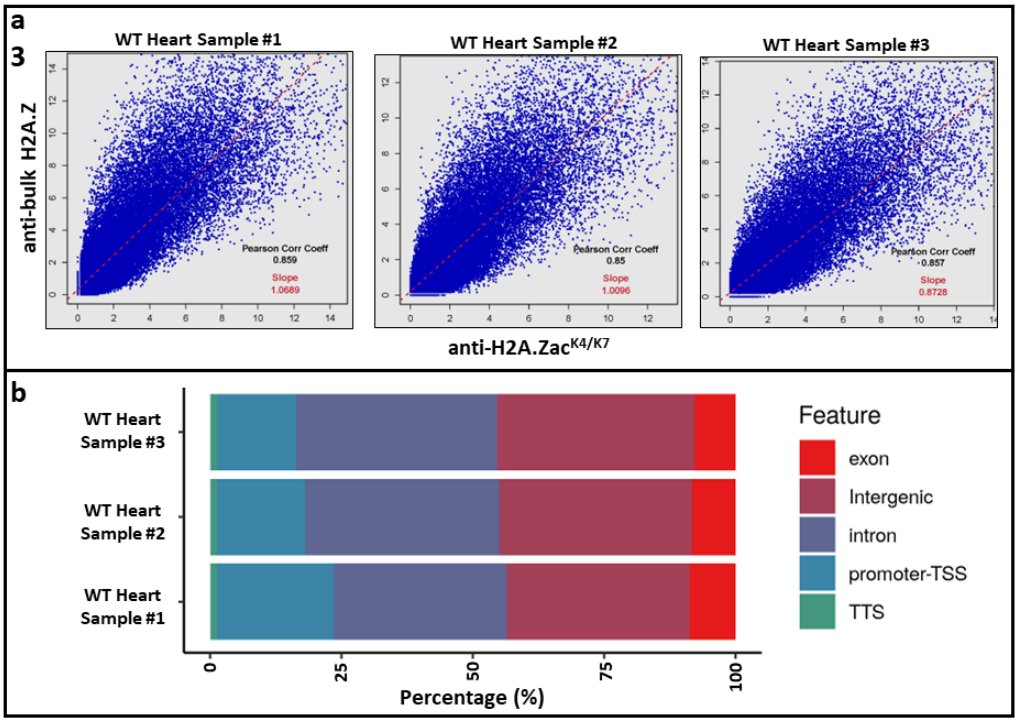

Supplemental Figure 8. CUT&Tag-based genomic localization of H2A.Zac$^{K4/K7}$. **Panel a:** Qualification of anti-H2A.Zac$^{K4/K7}$ antibody (Cell Signaling Technology #75336) for ability to perform CUT&Tag on adult heart tissue by comparing targets recognized by commercially-qualified antibody anti-bulk H2A.Z (Active Motif #39013). **Panel b:** Peak annotation analysis showing the percentages of H2A.Zac$^{K4/K7}$ peaks in genomic loci.

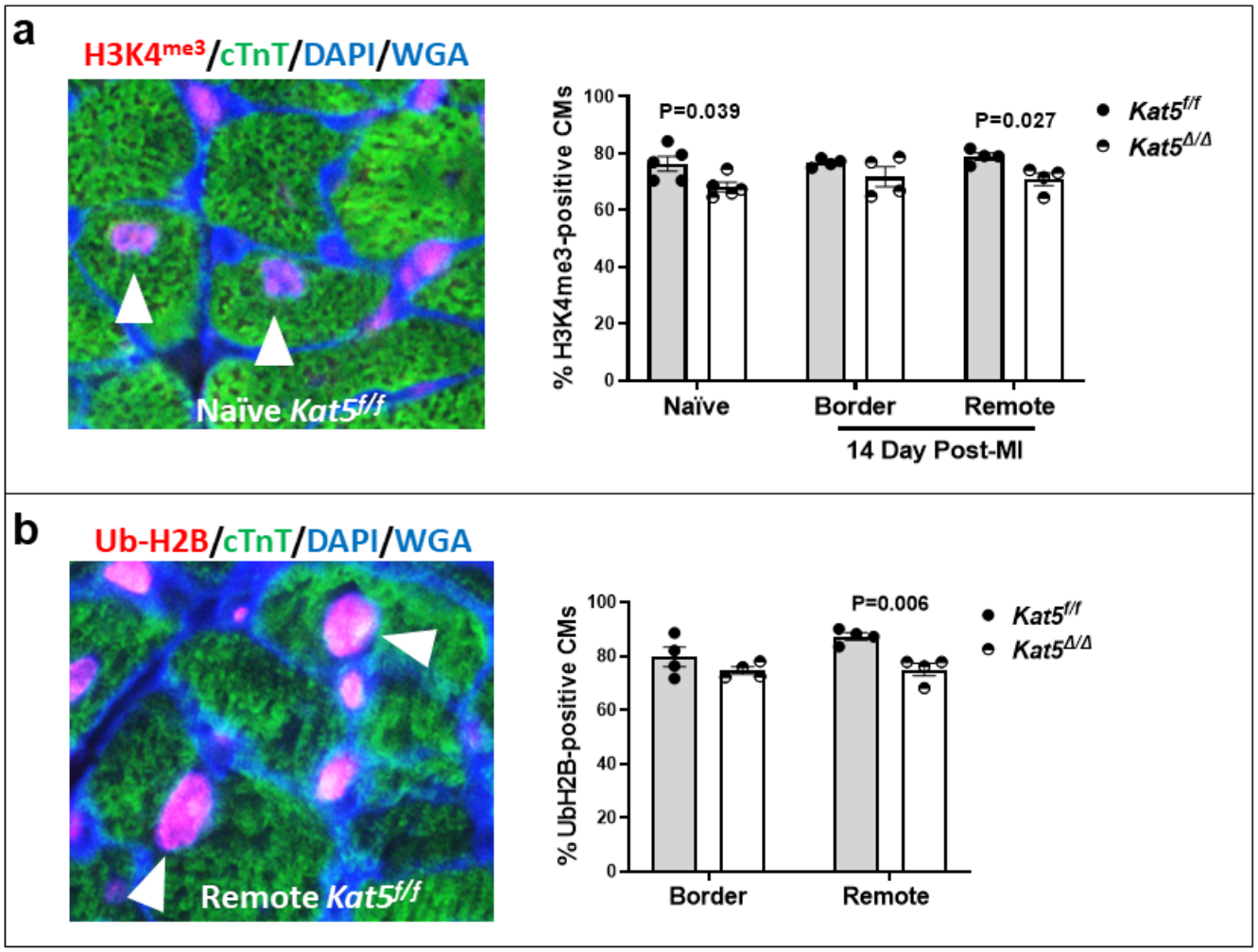

Supplemental Figure 9. Reduced Levels of Trimethylated Histone H3 (H3K4^{me3}) Ubiquitinated H2B in Tip60-depleted Hearts. Panel a, representative immunostained images showing H3K4^{me3}-positive CMs in 13-week-old adult hearts from which Tip60 was depleted in CMs. **Panel b**, Ub-H2B stained hearts. In both assessments, percentages of H3K4^{me3}- and Ub-H2B-positive CMs (white arrowheads) were determined by evaluating at least 300 CMs in six randomly selected 400x cross-sectional fields. Bars denote means ±SEM. *P<0.05 vs. *Kat5$^{f/f}$* per unpaired Student's t-test. Each point represents a biological replicate (i.e., an individual mouse heart).

REFERENCES

1. Tsao CW, Aday AW, Almarzooq ZI, Alonso A, Beaton AZ, Bittencourt MS, Boehme AK, Buxton AE, Carson AP, Commodore-Mensah Y, Elkind MSV, Evenson KR, Eze-Nliam C, Ferguson JF, Generoso G, Ho JE, Kalani R, Khan SS, Kissela BM, Knutson KL, Levine DA, Lewis TT, Liu J, Loop MS, Ma J, Mussolino ME, Navaneethan SD, Perak AM, Poudel R, Rezk-Hanna M, Roth GA, Schroeder EB, Shah SH, Thacker EL, VanWagner LB, Virani SS, Voecks JH, Wang NY, Yaffe K and Martin SS. Heart Disease and Stroke Statistics-2022 Update: A Report From the American Heart Association. *Circulation*. 2022;145:e153-e639.
2. Sadek H and Olson EN. Toward the Goal of Human Heart Regeneration. *Cell Stem Cell*. 2020;26:7-16.
3. Lee MS, Seo J, Choi DY, Lee EW, Ko A, Ha NC, Yoon JB, Lee HW, Kim KP and Song J. Stabilization of p21 (Cip1/WAF1) following Tip60-dependent acetylation is required for p21-mediated DNA damage response. *Cell death and differentiation*. 2013;20:620-9.
4. Li B, Hu Y, Li X, Jin G, Chen X, Chen G, Chen Y, Huang S, Liao W, Liao Y, Teng Z and Bin J. Sirt1 Antisense Long Noncoding RNA Promotes Cardiomyocyte Proliferation by Enhancing the Stability of Sirt1. *J Am Heart Assoc*. 2018;7:e009700.
5. Sun Y, Jiang X, Chen S, Fernandes N and Price BD. A role for the Tip60 histone acetyltransferase in the acetylation and activation of ATM. *Proc Natl Acad Sci U S A*. 2005;102:13182-7.
6. Bose A, Sudevan S, Rao VJ, Shima H, Trivedi AK, Igarashi K and Kundu TK. Haploinsufficient tumor suppressor Tip60 negatively regulates oncogenic Aurora B kinase. *J Biosci*. 2019;44.
7. Sykes SM, Mellert HS, Holbert MA, Li K, Marmorstein R, Lane WS and McMahon SB. Acetylation of the p53 DNA-binding domain regulates apoptosis induction. *Mol Cell*. 2006;24:841-51.
8. Tang Y, Luo J, Zhang W and Gu W. Tip60-dependent acetylation of p53 modulates the decision between cell-cycle arrest and apoptosis. *Mol Cell*. 2006;24:827-39.
9. Tang Y, Zhao W, Chen Y, Zhao Y and Gu W. Acetylation is indispensable for p53 activation. *Cell*. 2008;133:612-26.
10. Wang X, Lupton C, Lauth A, Wan TC, Foster P, Patterson M, Auchampach JA and Lough JW. Evidence that the acetyltransferase Tip60 induces the DNA damage response and cell-cycle arrest in neonatal cardiomyocytes. *J Mol Cell Cardiol*. 2021.
11. Wang X, Wan TC, Lauth A, Purdy AL, Kulik KR, Patterson M, Lough JW and Auchampach JA. Conditional depletion of the acetyltransferase Tip60 protects against the damaging effects of myocardial infarction. *J Mol Cell Cardiol*. 2022;163:9-19.
12. Wang X, Wan TC, Kulik KR, Lauth A, Smith BC, Lough JW and Auchampach JA. Pharmacological inhibition of the acetyltransferase Tip60 mitigates myocardial infarction injury. *Dis Model Mech*. 2023;16.
13. Kubin T, Poling J, Kostin S, Gajawada P, Hein S, Rees W, Wietelmann A, Tanaka M, Lorchner H, Schimanski S, Szibor M, Warnecke H and Braun T. Oncostatin M is a major mediator of cardiomyocyte dedifferentiation and remodeling. *Cell Stem Cell*. 2011;9:420-32.
14. D'Uva G, Aharonov A, Lauriola M, Kain D, Yahalom-Ronen Y, Carvalho S, Weisinger K, Bassat E, Rajchman D, Yifa O, Lysenko M, Konfino T, Hegesh J, Brenner O, Neeman M, Yarden Y, Leor J, Sarig R, Harvey RP and Tzahor E. ERBB2 triggers mammalian heart regeneration by promoting cardiomyocyte dedifferentiation and proliferation. *Nat Cell Biol*. 2015;17:627-38.
15. Valussi M, Besser J, Wystub-Lis K, Zukunft S, Richter M, Kubin T, Boettger T and Braun T. Repression of Osmr and Fgfr1 by miR-1/133a prevents cardiomyocyte dedifferentiation and cell cycle entry in the adult heart. *Sci Adv*. 2021;7:eabi6648.
16. Avraham Shakked ZP, Alla Aharonov, Matteo Ghiringhelli, Kfir-Baruch Umansky, David Kain, Jacob Elkahal, Yalin Divinsky, Phong Dang Nguyen, Shoval Miyara, Gilgi Friedlander, Alon Savidor, Lingling Zhang, Dahlia E. Perez, Rachel Sarig, Daria Lendengolts, Hanna Bueno-Levy, Nathaniel Kastan, Yishai Levin, Jeroen Bakkers, Lior Gepstein & Eldad Tzahor. Redifferentiated cardiomyocytes retain residual dedifferentiation signatures are are protected from ischemic injury. *Nature Cardiovascular Research*. 2023;2:383-398.
17. Yahalom-Ronen Y, Rajchman D, Sarig R, Geiger B and Tzahor E. Reduced matrix rigidity promotes neonatal cardiomyocyte dedifferentiation, proliferation and clonal expansion. *eLife*. 2015;4.
18. Li X, Wu F, Gunther S, Looso M, Kuenne C, Zhang T, Wiesnet M, Klatt S, Zukunft S, Fleming I, Poschet G, Wietelmann A, Atzberger A, Potente M, Yuan X and Braun T. Inhibition of fatty acid oxidation enables heart regeneration in adult mice. *Nature*. 2023;622:619-626.

19. Chen Y, Luttmann FF, Schoger E, Scholer HR, Zelarayan LC, Kim KP, Haigh JJ, Kim J and Braun T. Reversible reprogramming of cardiomyocytes to a fetal state drives heart regeneration in mice. *Science*. 2021;373:1537-1540.
20. Kubin T, Gajawada P, Bramlage P, Hein S, Berge B, Cetinkaya A, Burger H, Schonburg M, Schaper W, Choi YH and Richter M. The Role of Oncostatin M and Its Receptor Complexes in Cardiomyocyte Protection, Regeneration, and Failure. *International journal of molecular sciences*. 2022;23.
21. Sorbini M, Arab S, Soni T, Frisiras A and Mehta S. How can the adult zebrafish and neonatal mice teach us about stimulating cardiac regeneration in the human heart? *Regen Med*. 2023;18:85-99.
22. Yang X, Li L, Zeng C and Wang WE. The characteristics of proliferative cardiomyocytes in mammals. *J Mol Cell Cardiol*. 2023;185:50-64.
23. Beisaw A and Wu CC. Cardiomyocyte maturation and its reversal during cardiac regeneration. *Dev Dyn*. 2022.
24. Bassat E, Mutlak YE, Genzelinakh A, Shadrin IY, Baruch Umansky K, Yifa O, Kain D, Rajchman D, Leach J, Riabov Bassat D, Udi Y, Sarig R, Sagi I, Martin JF, Bursac N, Cohen S and Tzahor E. The extracellular matrix protein agrin promotes heart regeneration in mice. *Nature*. 2017;547:179-184.
25. Williams C, Quinn KP, Georgakoudi I and Black LD, 3rd. Young developmental age cardiac extracellular matrix promotes the expansion of neonatal cardiomyocytes in vitro. *Acta biomaterialia*. 2014;10:194-204.
26. Notari M, Ventura-Rubio A, Bedford-Guaus SJ, Jorba I, Mulero L, Navajas D, Marti M and Raya A. The local microenvironment limits the regenerative potential of the mouse neonatal heart. *Sci Adv*. 2018;4:eaao5553.
27. Numata A, Kwok HS, Zhou QL, Li J, Tirado-Magallanes R, Angarica VE, Hannah R, Park J, Wang CQ, Krishnan V, Rajagopalan D, Zhang Y, Zhou S, Welner RS, Osato M, Jha S, Bohlander SK, Gottgens B, Yang H, Benoukraf T, Lough JW, Bararia D and Tenen DG. Lysine acetyltransferase Tip60 is required for hematopoietic stem cell maintenance. *Blood*. 2020;136:1735-1747.
28. Janas JA, Zhang L, Luu JH, Demeter J, Meng L, Marro SG, Mall M, Mooney NA, Schaukowitch K, Ng YH, Yang N, Huang Y, Neumayer G, Gozani O, Elias JE, Jackson PK and Wernig M. Tip60-mediated H2A.Z acetylation promotes neuronal fate specification and bivalent gene activation. *Mol Cell*. 2022.
29. Fisher JB, Horst A, Wan T, Kim MS, Auchampach J and Lough J. Depletion of Tip60 from In Vivo Cardiomyocytes Increases Myocyte Density, Followed by Cardiac Dysfunction, Myocyte Fallout and Lethality. *PLoS One*. 2016;11:e0164855.
30. Sohal DS, Nghiem M, Crackower MA, Witt SA, Kimball TR, Tymitz KM, Penninger JM and Molkentin JD. Temporally regulated and tissue-specific gene manipulations in the adult and embryonic heart using a tamoxifen-inducible Cre protein. *Circ Res*. 2001;89:20-5.
31. Heinz S, Benner C, Spann N, Bertolino E, Lin YC, Laslo P, Cheng JX, Murre C, Singh H and Glass CK. Simple combinations of lineage-determining transcription factors prime cis-regulatory elements required for macrophage and B cell identities. *Mol Cell*. 2010;38:576-89.
32. Li D, Purushotham D, Harrison JK, Hsu S, Zhuo X, Fan C, Liu S, Xu V, Chen S, Xu J, Ouyang S, Wu AS and Wang T. WashU Epigenome Browser update 2022. *Nucleic Acids Res*. 2022;50:W774-W781.
33. Tzahor E and Dimmeler S. A coalition to heal-the impact of the cardiac microenvironment. *Science*. 2022;377:eabm4443.
34. Bouhamida E, Vadakke-Madathil S, Mathiyalagan P, Ranjan AK, Sherman CD, Miller PE, Ghetti A, Abi-Gerges N and Chaudhry HW. Single nucleus transcriptomics supports a role for CCNA2-induced human adult cardiomyocyte cytokinesis. *bioRxiv*. 2024.
35. Tabula Muris C, Overall c, Logistical c, Organ c, processing, Library p, sequencing, Computational data a, Cell type a, Writing g, Supplemental text writing g and Principal i. Single-cell transcriptomics of 20 mouse organs creates a Tabula Muris. *Nature*. 2018;562:367-372.
36. Aharonov A, Shakked A, Umansky KB, Savidor A, Genzelinakh A, Kain D, Lendengolts D, Revach OY, Morikawa Y, Dong J, Levin Y, Geiger B, Martin JF and Tzahor E. ERBB2 drives YAP activation and EMT-like processes during cardiac regeneration. *Nat Cell Biol*. 2020;22:1346-1356.
37. Fan X, Hughes BG, Ali MA, Cho WJ, Lopez W and Schulz R. Dynamic Alterations to alpha-Actinin Accompanying Sarcomere Disassembly and Reassembly during Cardiomyocyte Mitosis. *PLoS One*. 2015;10:e0129176.
38. Sun Y, Sun J, Lungchukiet P, Quarni W, Yang S, Zhang X and Bai W. Fe65 Suppresses Breast Cancer Cell Migration and Invasion through Tip60 Mediated Cortactin Acetylation. *Sci Rep*. 2015;5:11529.

39. Ammer AG and Weed SA. Cortactin branches out: roles in regulating protrusive actin dynamics. *Cell Motil Cytoskeleton*. 2008;65:687-707.
40. Ren G, Crampton MS and Yap AS. Cortactin: Coordinating adhesion and the actin cytoskeleton at cellular protrusions. *Cell Motil Cytoskeleton*. 2009;66:865-73.
41. Hertig V, Matos-Nieves A, Garg V, Villeneuve L, Mamarbachi M, Caland L and Calderone A. Nestin expression is dynamically regulated in cardiomyocytes during embryogenesis. *J Cell Physiol*. 2018;233:3218-3229.
42. Herrer I, Rosello-Lleti E, Rivera M, Molina-Navarro MM, Tarazon E, Ortega A, Martinez-Dolz L, Trivino JC, Lago F, Gonzalez-Juanatey JR, Bertomeu V, Montero JA and Portoles M. RNA-sequencing analysis reveals new alterations in cardiomyocyte cytoskeletal genes in patients with heart failure. *Lab Invest*. 2014;94:645-53.
43. Chang AN, Mahajan P, Knapp S, Barton H, Sweeney HL, Kamm KE and Stull JT. Cardiac myosin light chain is phosphorylated by Ca2+/calmodulin-dependent and -independent kinase activities. *Proc Natl Acad Sci U S A*. 2016;113:E3824-33.
44. Sugi Y and Lough J. Onset of expression and regional deposition of alpha-smooth and sarcomeric actin during avian heart development. *Dev Dyn*. 1992;193:116-24.
45. Durbin MD, O'Kane J, Lorentz S, Firulli AB and Ware SM. SHROOM3 is downstream of the planar cell polarity pathway and loss-of-function results in congenital heart defects. *Dev Biol*. 2020;464:124-136.
46. Bedada FB, Chan SS, Metzger SK, Zhang L, Zhang J, Garry DJ, Kamp TJ, Kyba M and Metzger JM. Acquisition of a quantitative, stoichiometrically conserved ratiometric marker of maturation status in stem cell-derived cardiac myocytes. *Stem Cell Reports*. 2014;3:594-605.
47. VanDusen NJ, Lee JY, Gu W, Butler CE, Sethi I, Zheng Y, King JS, Zhou P, Suo S, Guo Y, Ma Q, Yuan GC and Pu WT. Massively parallel in vivo CRISPR screening identifies RNF20/40 as epigenetic regulators of cardiomyocyte maturation. *Nature communications*. 2021;12:4442.
48. Itou J, Oishi I, Kawakami H, Glass TJ, Richter J, Johnson A, Lund TC and Kawakami Y. Migration of cardiomyocytes is essential for heart regeneration in zebrafish. *Development*. 2012;139:4133-42.
49. Zhang R, Han P, Yang H, Ouyang K, Lee D, Lin YF, Ocorr K, Kang G, Chen J, Stainier DY, Yelon D and Chi NC. In vivo cardiac reprogramming contributes to zebrafish heart regeneration. *Nature*. 2013;498:497-501.
50. Morikawa Y, Zhang M, Heallen T, Leach J, Tao G, Xiao Y, Bai Y, Li W, Willerson JT and Martin JF. Actin cytoskeletal remodeling with protrusion formation is essential for heart regeneration in Hippo-deficient mice. *Science signaling*. 2015;8:ra41.
51. Kuhn B, del Monte F, Hajjar RJ, Chang YS, Lebeche D, Arab S and Keating MT. Periostin induces proliferation of differentiated cardiomyocytes and promotes cardiac repair. *Nat Med*. 2007;13:962-9.
52. Luxan G and Dimmeler S. The vasculature: a therapeutic target in heart failure? *Cardiovasc Res*. 2022;118:53-64.
53. Rasi K, Piuhola J, Czabanka M, Sormunen R, Ilves M, Leskinen H, Rysa J, Kerkela R, Janmey P, Heljasvaara R, Peuhkurinen K, Vuolteenaho O, Ruskoaho H, Vajkoczy P, Pihlajaniemi T and Eklund L. Collagen XV is necessary for modeling of the extracellular matrix and its deficiency predisposes to cardiomyopathy. *Circ Res*. 2010;107:1241-52.
54. Rhee S, Paik DT, Yang JY, Nagelberg D, Williams I, Tian L, Roth R, Chandy M, Ban J, Belbachir N, Kim S, Zhang H, Phansalkar R, Wong KM, King DA, Valdez C, Winn VD, Morrison AJ, Wu JC and Red-Horse K. Endocardial/endothelial angiocrines regulate cardiomyocyte development and maturation and induce features of ventricular non-compaction. *Eur Heart J*. 2021;42:4264-4276.
55. Baehr A, Umansky KB, Bassat E, Jurisch V, Klett K, Bozoglu T, Hornaschewitz N, Solyanik O, Kain D, Ferraro B, Cohen-Rabi R, Krane M, Cyran C, Soehnlein O, Laugwitz KL, Hinkel R, Kupatt C and Tzahor E. Agrin Promotes Coordinated Therapeutic Processes Leading to Improved Cardiac Repair in Pigs. *Circulation*. 2020;142:868-881.
56. Inai K. Atrioventricular Valve Abnormalities: From Molecular Mechanisms Underlying Morphogenesis to Clinical Perspective. In: T. Nakanishi, R. R. Markwald, H. S. Baldwin, B. B. Keller, D. Srivastava and H. Yamagishi, eds. *Etiology and Morphogenesis of Congenital Heart Disease: From Gene Function and Cellular Interaction to Morphology* Tokyo; 2016: 135-43.
57. Stohn JP, Perreault NG, Wang Q, Liaw L and Lindner V. Cthrc1, a novel circulating hormone regulating metabolism. *PLoS One*. 2012;7:e47142.

58. Nordquist EM, Dutta P, Kodigepalli KM, Mattern C, McDermott MR, Trask AJ, LaHaye S, Lindner V and Lincoln J. Tgfbeta1-Cthrc1 Signaling Plays an Important Role in the Short-Term Reparative Response to Heart Valve Endothelial Injury. *Arteriosclerosis, thrombosis, and vascular biology*. 2021;41:2923-2942.
59. Ruiz-Villalba A, Romero JP, Hernandez SC, Vilas-Zornoza A, Fortelny N, Castro-Labrador L, San Martin-Uriz P, Lorenzo-Vivas E, Garcia-Olloqui P, Palacio M, Gavira JJ, Bastarrika G, Janssens S, Wu M, Iglesias E, Abizanda G, de Morentin XM, Lasaga M, Planell N, Bock C, Alignani D, Medal G, Prudovsky I, Jin YR, Ryzhov S, Yin H, Pelacho B, Gomez-Cabrero D, Lindner V, Lara-Astiaso D and Prosper F. Single-Cell RNA Sequencing Analysis Reveals a Crucial Role for CTHRC1 (Collagen Triple Helix Repeat Containing 1) Cardiac Fibroblasts After Myocardial Infarction. *Circulation*. 2020;142:1831-1847.
60. Maroli G and Braun T. The long and winding road of cardiomyocyte maturation. *Cardiovasc Res*. 2021;117:712-726.
61. Honkoop H, de Bakker DE, Aharonov A, Kruse F, Shakked A, Nguyen PD, de Heus C, Garric L, Muraro MJ, Shoffner A, Tessadori F, Peterson JC, Noort W, Bertozzi A, Weidinger G, Posthuma G, Grun D, van der Laarse WJ, Klumperman J, Jaspers RT, Poss KD, van Oudenaarden A, Tzahor E and Bakkers J. Single-cell analysis uncovers that metabolic reprogramming by ErbB2 signaling is essential for cardiomyocyte proliferation in the regenerating heart. *eLife*. 2019;8.
62. Bae J, Salamon RJ, Brandt EB, Paltzer WG, Zhang Z, Britt EC, Hacker TA, Fan J and Mahmoud AI. Malonate Promotes Adult Cardiomyocyte Proliferation and Heart Regeneration. *Circulation*. 2021;143:1973-1986.
63. Shi Y, Tian M, Zhao X, Tang L, Wang F, Wu H, Liao Q, Ren H, Fu W, Zheng S, Jose PA, Li L and Zeng C. alpha-Ketoglutarate promotes cardiomyocyte proliferation and heart regeneration after myocardial infarction. *Nat Cardiovasc Res*. 2024;3:1083-1097.
64. Janas JA, Zhang L, Luu JH, Demeter J, Meng L, Marro SG, Mall M, Mooney NA, Schaukowitch K, Ng YH, Yang N, Huang Y, Neumayer G, Gozani O, Elias JE, Jackson PK and Wernig M. Tip60-mediated H2A.Z acetylation promotes neuronal fate specification and bivalent gene activation. *Mol Cell*. 2022;82:4627-4646 e14.
65. Wichmann J, Pitt C, Eccles S, Garnham AL, Li-Wai-Suen CSN, May R, Allan E, Wilcox S, Herold MJ, Smyth GK, Monahan BJ, Thomas T and Voss AK. Loss of TIP60 (KAT5) abolishes H2AZ lysine 7 acetylation and causes p53, INK4A, and ARF-independent cell cycle arrest. *Cell death & disease*. 2022;13:627.
66. Hirose K, Payumo AY, Cutie S, Hoang A, Zhang H, Guyot R, Lunn D, Bigley RB, Yu H, Wang J, Smith M, Gillett E, Muroy SE, Schmid T, Wilson E, Field KA, Reeder DM, Maden M, Yartsev MM, Wolfgang MJ, Grutzner F, Scanlan TS, Szweda LI, Buffenstein R, Hu G, Flamant F, Olgin JE and Huang GN. Evidence for hormonal control of heart regenerative capacity during endothermy acquisition. *Science*. 2019;364:184-188.
67. Payumo AY, Chen X, Hirose K, Chen X, Hoang A, Khyeam S, Yu H, Wang J, Chen Q, Powers N, Chen L, Bigley RB, Lovas J, Hu G and Huang GN. Adrenergic-Thyroid Hormone Interactions Drive Postnatal Thermogenesis and Loss of Mammalian Heart Regenerative Capacity. *Circulation*. 2021;144:1000-1003.
68. Zhou P, VanDusen NJ, Zhang Y, Cao Y, Sethi I, Hu R, Zhang S, Wang G, Ye L, Mazumdar N, Chen J, Zhang X, Guo Y, Li B, Ma Q, Lee JY, Gu W, Yuan GC, Ren B, Chen K and Pu WT. Dynamic changes in P300 enhancers and enhancer-promoter contacts control mouse cardiomyocyte maturation. *Dev Cell*. 2023;58:898-914 e7.
69. Murphy SA, Miyamoto M, Kervadec A, Kannan S, Tampakakis E, Kambhampati S, Lin BL, Paek S, Andersen P, Lee DI, Zhu R, An SS, Kass DA, Uosaki H, Colas AR and Kwon C. PGC1/PPAR drive cardiomyocyte maturation at single cell level via YAP1 and SF3B2. *Nature communications*. 2021;12:1648.
70. Liu Y, Bai H, Guo F, Thai PN, Luo X, Zhang P, Yang C, Feng X, Zhu D, Guo J, Liang P, Xu Z, Yang H and Lu X. PGC-1alpha activator ZLN005 promotes maturation of cardiomyocytes derived from human embryonic stem cells. *Aging (Albany NY)*. 2020;12:7411-7430.
71. Zhang L, Zhang M, Huang J, Huang J, Zhang Y, Zhang Y, Chen H, Wang C, Xi X, Fan H, Wang J, Jiang D, Tian J, Zhang J and Chang Y. Klf9 is essential for cardiac mitochondrial homeostasis. *Nat Cardiovasc Res*. 2024;3:1318-1336.
72. Kao YR, Chen J, Kumari R, Ng A, Zintiridou A, Tatiparthy M, Ma Y, Aivalioti MM, Moulik D, Sundaravel S, Sun D, Reisz JA, Grimm J, Martinez-Lopez N, Stransky S, Sidoli S, Steidl U, Singh R, D'Alessandro A and Will B. An iron rheostat controls hematopoietic stem cell fate. *Cell Stem Cell*. 2024;31:378-397 e12.
73. Yang Z, Mameri A, Cattoglio C, Lachance C, Florez Ariza AJ, Luo J, Humbert J, Sudarshan D, Banerjea A, Galloy M, Fradet-Turcotte A, Lambert JP, Ranish JA, Cote J and Nogales E. Structural insights into the human NuA4/TIP60 acetyltransferase and chromatin remodeling complex. *Science*. 2024;385:eadl5816.

74. Law C and Cheung P. Expression of Non-acetylatable H2A.Z in Myoblast Cells Blocks Myoblast Differentiation through Disruption of MyoD Expression. *J Biol Chem*. 2015;290:13234-49.
75. Narkaj K, Stefanelli G, Wahdan M, Azam AB, Ramzan F, Steininger CFD, Jr., Walters BJ and Zovkic IB. Blocking H2A.Z Incorporation via Tip60 Inhibition Promotes Systems Consolidation of Fear Memory in Mice. *eNeuro*. 2018;5.
76. Yao F, Yu P, Li Y, Yuan X, Li Z, Zhang T, Liu F, Wang Y, Wang Y, Li D, Ma B, Shu C, Kong W, Zhou B and Wang L. Histone Variant H2A.Z Is Required for the Maintenance of Smooth Muscle Cell Identity as Revealed by Single-Cell Transcriptomics. *Circulation*. 2018;138:2274-2288.
77. Giaimo BD, Ferrante F, Herchenrother A, Hake SB and Borggrefe T. The histone variant H2A.Z in gene regulation. *Epigenetics & chromatin*. 2019;12:37.
78. Tominaga K, Sakashita E, Kasashima K, Kuroiwa K, Nagao Y, Iwamori N and Endo H. Tip60/KAT5 Histone Acetyltransferase Is Required for Maintenance and Neurogenesis of Embryonic Neural Stem Cells. *International journal of molecular sciences*. 2023;24.
79. Ikeda S, Mizushima W, Sciarretta S, Abdellatif M, Zhai P, Mukai R, Fefelova N, Oka SI, Nakamura M, Del Re DP, Farrance I, Park JY, Tian B, Xie LH, Kumar M, Hsu CP, Sadayappan S, Shimokawa H, Lim DS and Sadoshima J. Hippo Deficiency Leads to Cardiac Dysfunction Accompanied by Cardiomyocyte Dedifferentiation During Pressure Overload. *Circ Res*. 2019;124:292-305.
80. Zhu Y, Do VD, Richards AM and Foo R. What we know about cardiomyocyte dedifferentiation. *J Mol Cell Cardiol*. 2021;152:80-91.
81. Bongiovanni C, Sacchi F, Da Pra S, Pantano E, Miano C, Morelli MB and D'Uva G. Reawakening the Intrinsic Cardiac Regenerative Potential: Molecular Strategies to Boost Dedifferentiation and Proliferation of Endogenous Cardiomyocytes. *Front Cardiovasc Med*. 2021;8:750604.
82. Uscategui Calderon M, Gonzalez BA and Yutzey KE. Cardiomyocyte-fibroblast crosstalk in the postnatal heart. *Front Cell Dev Biol*. 2023;11:1163331.
83. Durmus T, LeClair RJ, Park KS, Terzic A, Yoon JK and Lindner V. Expression analysis of the novel gene collagen triple helix repeat containing-1 (Cthrc1). *Gene Expr Patterns*. 2006;6:935-40.
84. Liu YJ, Du J, Li J, Tan XP and Zhang Q. CTHRC1, a novel gene with multiple functions in physiology, disease and solid tumors (Review). *Oncol Lett*. 2023;25:266.
85. Pyagay P, Heroult M, Wang Q, Lehnert W, Belden J, Liaw L, Friesel RE and Lindner V. Collagen triple helix repeat containing 1, a novel secreted protein in injured and diseased arteries, inhibits collagen expression and promotes cell migration. *Circ Res*. 2005;96:261-8.
86. Elia A, Mohsin S and Khan M. Cardiomyocyte Ploidy, Metabolic Reprogramming and Heart Repair. *Cells*. 2023;12.
87. Liao R, Jain M, Cui L, D'Agostino J, Aiello F, Luptak I, Ngoy S, Mortensen RM and Tian R. Cardiac-specific overexpression of GLUT1 prevents the development of heart failure attributable to pressure overload in mice. *Circulation*. 2002;106:2125-31.
88. Tang Z, Wang K, Lo L and Chen J. Tg(Delta113p53:cmyc) Transgene Upregulates glut1 Expression to Promote Zebrafish Heart Regeneration. *J Cardiovasc Dev Dis*. 2023;10.
89. Fajardo VM, Feng I, Chen BY, Perez-Ramirez CA, Shi B, Clark P, Tian R, Lien CL, Pellegrini M, Christofk H, Nakano H and Nakano A. GLUT1 overexpression enhances glucose metabolism and promotes neonatal heart regeneration. *Sci Rep*. 2021;11:8669.
90. Auchampach J, Han L, Huang GN, Kuhn B, Lough JW, O'Meara CC, Payumo AY, Rosenthal NA, Sucov HM, Yutzey KE and Patterson M. Measuring cardiomyocyte cell-cycle activity and proliferation in the age of heart regeneration. *Am J Physiol Heart Circ Physiol*. 2022;322:H579-H596.
91. Swift SK, Purdy AL, Buddell T, Lovett JJ, Chanjeevaram SV, Arkatkar A, O'Meara CC and Patterson M. A broadly applicable method for quantifying cardiomyocyte cell division identifies proliferative events following myocardial infarction. *Cell Rep Methods*. 2024:100860.
92. Xuan F, Xuan H, Huang M, He W, Xu H, Shi X and Wen H. The Tudor-knot Domain of KAT5 Regulates Nucleosomal Substrate Acetylation. *Journal of molecular biology*. 2024;436:168414.
93. Wang X, Lauth A, Wan TC, Lough JW and Auchampach JA. Myh6-driven Cre-recombinase activates the DNA damage response and the cell-cycle in the myocardium in the absence of loxP sites. *Dis Model Mech*. 2020.